Eringen's Nonlocal and Modified Couple Stress Theories Applied to Vibrating Rotating Nanobeams with Temperature Effects

A. Rahmani[1], S. Faroughi[1], M.I. Friswell[2] and A. Babaei[3]

[1] *Faculty of Mechanical Engineering, Urmia University of Technology, Urmia, Iran*

[2] *College of Engineering, Swansea University, Swansea, UK*

[3] *Department of Mechanical Engineering, University of Kentucky, Lexington, Kentucky, USA*

[2*] Corresponding author, M. I. Friswell, Professor, E-mail: m.i.friswell@swansea.ac.uk

Eringen's Nonlocal and Modified Couple Stress Theories Applied to Vibrating Rotating Nanobeams with Temperature Effects

This study develops a comprehensive vibrational analysis of rotating nanobeams on visco-elastic foundations with thermal effects based on the modified couple stress and Eringen's nonlocal elasticity theories. This approach accurately simulates the nonlocal stress and size effects. Higher-order shear deformation beam theory and the generalized differential quadrature method are used to obtain the numerical results. The effects of nonlocal parameters, length scale, Winkler-Pasternak coefficients, thermal gradient, slenderness ratios, rotating velocity and viscoelastic coefficient are demonstrated and discussed in detail. Mode switching and the importance of the correct choice of theory and associated size effect parameters are highlighted.

Keywords: Eringen's Nonlocal Theory (ENT); Modified Couple Stress Theory (MCST); Thermal Effects; Rotating Nanobeam; Vibrational Behavior; Visco-Elastic Foundation

1. Introduction

In the past decade, applications of small-scale systems, such as micro/nano structures, have increased progressively because of their outstanding electrical, thermal and mechanical properties. Accordingly, the accurate evaluation and detailed study of mechanical behavior, such as bending [1, 2], buckling [3, 4], vibration [5-7] and wave propagation [8, 9] of nanostructures, is vital to increase the reliability and achieve the proper design of these small-scale systems. Due to the deficiency of classical theories of continuum mechanics to analyse the mechanical behavior of micro/nano structures, modified elasticity theories such as strain gradient elasticity, couple stress, Eringen's nonlocal elasticity and general nonlocal elasticity [10-20] have been proposed to resolve the problem. Many researchers have considered the static and dynamic analysis of micro/nano structures in recent years. Also, the effect of visco-elasticity on the dynamic behavior of structures have been considered extensively [21-23]. Moreover, the

application of computational methods to obtain the numerical results is important and has attracted many researchers. Some of the important, practical and novel computational methods employed in analysis of small-scale structures include the finite element method [24], the boundary element method [25], the differential quadrature method [26] and isogeometric analysis [27, 28].

The following literature review concentrates on the vibrational behavior, design and analysis of such small-scale micro/nano structural elements in recent years.

Zhen et al. [29] expressed the free vibration behavior of viscoelastic nanotubes under magnetic effects via nonlocal strain gradient theory (SGT) and Timoshenko beam theory (TBT). They applied a local adaptive differential quadrature method to calculate the numerical results. Babaei and Rahmani [30] investigated the lateral vibration of microbeams under thermal stresses based on Modified Couple Stress Theory (MCST) and TBT. Ansari et al. [31] employed surface stress elasticity theory to study the nonlinear forced vibration of nanobeams, and applied the generalized differential quadrature method (GDQM) and a Galerkin-based numerical approach to obtain the results. Şimşek [32] considered the dynamic analysis and vibrational behavior of a single-walled carbon nanotube including transverse shear deformation and rotary inertia using nonlocal TBT. Gao et al. [33] employed nonlocal SGT with a perturbation method to develop the nonlinear vibration analysis of functionally graded (FG) beams.

Rajasekaran and Khaniki [34] applied nonlocal SGT to study the mechanical behavior of non-uniform axially FG material (FGM) Euler-Bernoulli nanobeams. They employed the finite element (FE) and quadrature methods with Lagrangian multipliers to obtain their results. Aria and Friswell [35] investigated a nonlocal FE model for the buckling and free vibrational behavior of nanobeams based on a first-order shear deformation beam model. Trinh et al. [36] studied the free vibrational behavior of two-

directional microbeams with various boundary conditions. Their model was developed on the basis of MCST and quasi-3D theory. Ebrahimi and Barati considered the vibration of FG nanobeams [37] and flexoelectric nanobeams [38]. Mirjavadi et al. [39] presented the effects of porosity and temperature on the vibrational behavior of bi-directional FG microbeams using MCST and TBT. Ghandourah and Abdraboh [40] employed FEM for vibration analysis of FG porous nanobeams. They derived the model based on the Eringen nonlocal and Euler-Bernoulli beam theories. Roque et al. [41] studied the influence of small-scale parameters on the vibrational behavior of Timoshenko FGM nanobeams.

Shafiei et al. [42] investigated the vibrational behavior of bi-dimensional FG nanobeams applying both couple stress and Eringen's theory separately. They considered two different kinds of porous materials with various boundary conditions. Babaei et al. [43] reported the dynamic responses of oscillatory small-scale beams based on Eringen's nonlocal theory. The model included thermal stress due to a sudden temperature rise applied to the system through the top and bottom surfaces. Yuan et al. [44] presented the vibrational behavior of FG mono-layered non-uniform nanorods on the basis of the elasticity theories of Eringen and Gurtin-Murdoch and used the Galerkin method for the numerical calculations. Rotating nanostructures including micro/nano multiple gear systems, micro/nano gears, micro/nano turbines and micro/nano blades have been considered by the research community [45, 46]. The examination of vibration and wave propagation of nano-machines is important for their accurate design. Ansari and Torabi [47] employed nonlocal elasticity and first-order shear deformation theory to study the vibrational behavior of nanocones (CNCs) resting on an elastic foundation. They considered generalized differential quadrature and periodic differential operators to solve the problem. Khaniki [48] applied mixed local/nonlocal Eringen elasticity to study the transverse vibration behavior of rotating Euler-Bernoulli cantilevers.

Arvin [49] considered the flap-wise bending free vibrational behavior of rotating microbeams based on MCST and TBT via the differential transform method. Babaei and Yang [50] considered rotation effects from a kinetics view point. They utilized nonlocal Eringen's theory along with subtle kinetics based on the modified coupled displacement fields. Aranda-Ruiz et al. [51] investigated the free vibration of rotating non-uniform nano-cantilevers by applying Eringen's nonlocal theory (ENT). They considered the effects of the nonlocal small-scale, angular speed on the vibrational behavior of the nanobeam. Ghadiri and Shafiei [52] studied the nonlinear bending vibration of nonlocal Euler–Bernoulli nanobeams. Pradhan and Murmu [53] studied the flap-wise bending and vibration behavior of rotating clamped-free nanobeams based on Eringen's model. Fang et al. [54, 55] established three-dimensional models of rotating FG small scale beams using MCST and an Euler–Bernoulli beam model. They utilized Lagrange's equations and a Ritz method to model and analyze the axial, chord-wise, and flap-wise motions. Bhattacharya and Das [56] presented the free vibrational behavior of bi-directional FG double-tapered rotating micro-beams. They developed the model on the basis of TBT and MSCT.

Yin et al. [57] developed a new isogeometric Timoshenko beam model to study static bending and free vibration of micro-beams using MCST and surface elasticity theory. They employed a novel computational approach based on isogeometric analysis. Norouzzadeh et al. [58] studied the nonlinear bending analysis of nanobeams using a comprehensive nonlocal strain gradient Timoshenko beam model without any simplification. Also, they proposed a non-classical isogeometric analysis to obtain the numerical results.

Ehyaei et al. [59] expressed the effects of porosity and preload on the vibration characteristics of rotating FG nanobeams. They used ENT and Euler–Bernoulli beam

model in their research. Ebrahimi and Shafei [60] expressed the vibrational behavior of rotating FG nano-beams via ENT. Rouhi et al. [61] studied nonlinear free and forced vibration of nanobeams. They employed Mindlin's second strain gradient theory to investigate the size effects and Timoshenko beam theory to extract the model. They used variational differential quadrature to obtain the numerical results. Azimi et al. [62] considered the vibrational behavior of rotating clamped-free FG nano-beams based on ENT and TBT under nonlinear thermal distribution. Vibrational studies of rotating nanobeams including the effects of the elastic foundation and the thermal environment were reported by Mohammadi et al. [63]. Talebitooti et al. [64] considered the semi-analytical vibration analysis of a rotating tapered axially FG nanobeam using ENT and a differential transformation method to extract the numerical results.

According to the above literature review, the existing investigations on the vibrational behavior in small-scaled beams are chiefly based on ENT, SGT and MCST but a clear gap is the difference in their applications, and the most appropriate theory to employ in specific cases. Hence, in this study, the model of a nanobeam is developed using both Eringen's nonlocal and modified couple stress theories with two different scale parameters to capture size effects. In the current research, the model is established based on MCST to include the effect of local rotational DOF. Also, this model is developed in the framework of ENT which captures nonlocal and long-range interactions between particles. In fact, to capture both hardening and softening behavior of materials, both Eringen's nonlocal and the modified couple stress theories are considered. Then, GDQM is applied to the both models to obtain the numerical results. Furthermore, this comprehensive study includes interactions due to rotation, thermal and viscoelastic foundation effects in a higher-order-shear deformation beam model for the first time.

2. Model Formulation

2.1. Description

Figure 1 shows a rotating nanobeam resting on a visco-elastic Winkler-Pasternak foundation incorporating thermal effects. The nanobeam has length L and a rectangular cross section with thickness h and width b.

Figure 1

2.2. Modified Couple Stress Theory (MCST)

Based on the modified couple stress theory [17], the strain energy density, Π_s, is given in terms of both the strain and curvature conjugated with the stress and couple stress respectively, as

$$\Pi_s = \int_0^L \int_A (\boldsymbol{\sigma}: \boldsymbol{\varepsilon} + \boldsymbol{m}: \boldsymbol{\chi}) dA dx \tag{1}$$

where $\boldsymbol{\sigma}, \boldsymbol{\varepsilon}, \boldsymbol{\chi}$ and $\boldsymbol{m}$ are the stress, strain, curvature tensors and the deviatoric part of the couple stress tensor respectively and the (i,j) elements of these tensors are given by

$$\sigma_{ij} = \lambda \varepsilon_{rr} \delta_{ij} + 2G\varepsilon_{ij} \tag{2}$$

$$\varepsilon_{ij} = \frac{1}{2}\left(u_{i,j} + u_{j,i}\right) \tag{3}$$

$$\chi_{ij} = \frac{1}{2}\left(\theta_{i,j} + \theta_{j,i}\right) \tag{4}$$

$$m_{ij} = 2\mu l_m^2 \chi_{ij} \tag{5}$$

where $i, j = 1, 2, 3$ represent the x, y and z directions. Also, λ and G are Lame's constants, $\boldsymbol{u}$ and $\boldsymbol{\theta}$ are displacement and rotation vectors respectively and l_m is the material length scale parameter. δ_{ij} is the Kronecker delta. The relationship between $\boldsymbol{u}$ and $\boldsymbol{\theta}$ is expressed as

$$\boldsymbol{\theta} = \frac{1}{2}\mathrm{curl}(\boldsymbol{u}) \tag{6}$$

In the current study, third shear deformation theory (Reddy beam) is applied to represent the kinematic model of the nano-beam resting on a viscoelastic Winkler-Pasternak foundation. The displacement field $\boldsymbol{u} = (u_1, u_2, u_3)$ is described as

$$u_1 = u + z\varphi - c_1 z^3(\varphi + \frac{\partial w}{\partial x}); \qquad u_2 = 0; \qquad u_3 = w \tag{7}$$

where u and w are the longitudinal and transverse displacement, φ is the rotation of the cross section at the neutral axis and $c_1 = 4/(3h^2)$. The strains in the Reddy beam model are defined as

$$\varepsilon_{xx} = \frac{\partial u_1}{\partial x} = \frac{\partial u}{\partial x} + z\frac{\partial \varphi}{\partial x} - c_1 z^3(\frac{\partial \varphi}{\partial x} + \frac{\partial^2 w}{\partial x^2}) \tag{8-a}$$

$$2\varepsilon_{xz} = \frac{\partial u_1}{\partial z} + \frac{\partial u_3}{\partial x} = (\varphi + \frac{\partial w}{\partial x}) - c_2 z^2(\varphi + \frac{\partial w}{\partial x}) \tag{8-b}$$

From Eqs. (4)-(7):

$$2\chi_{yx} = \frac{1}{2}\left(\frac{\partial \varphi}{\partial x} - \frac{\partial^2 w}{\partial x^2} - c_2 z^2(\frac{\partial \varphi}{\partial x} + \frac{\partial^2 w}{\partial x^2})\right) \tag{9-a}$$

$$2\chi_{yz} = -c_2 z(\varphi + \frac{\partial w}{\partial x}) \tag{9-b}$$

where $c_2 = 3c_1$.

Thus, substituting Eqs. (2) - (5) into Eq. (1), and applying some algebraic simplifications, the strain energy density becomes

$$\Pi_s = \int_0^L \left[\begin{array}{l} M_{xx}^{(0)}\frac{\partial u}{\partial x} + M_{xx}^{(1)}\frac{\partial \varphi}{\partial x} - c_1 M_{xx}^{(3)}(\frac{\partial \varphi}{\partial x} + \frac{\partial^2 w}{\partial x^2}) + Q_{xz}^{(0)}(\varphi + \frac{\partial w}{\partial x}) - c_2 Q_{xz}^{(2)}(\varphi + \frac{\partial w}{\partial x}) + \\ \frac{1}{2}Y_{yx}^{(0)}(\frac{\partial \varphi}{\partial x} - \frac{\partial^2 w}{\partial x^2}) - \frac{c_2}{2}Y_{yx}^{(2)}(\frac{\partial \varphi}{\partial x} + \frac{\partial^2 w}{\partial x^2}) - c_2 Y_{yz}^{(1)}(\varphi + \frac{\partial w}{\partial x}) \end{array}\right] dx \tag{10}$$

where

$$M_{xx}^{(i)} = \int_A \sigma_{xx} z^i dA\,; \qquad Q_{xz}^{(i)} = \int_A \sigma_{xz} z^i\, dA \tag{11-a}$$

$$Y_{yx}^{(i)} = \int_A m_{yx} z^i dA\,; \qquad Y_{yz}^{(i)} = \int_A m_{yz} z^i\, dA \tag{11-b}$$

and $i = 0,1,2,3$.

2.2.1. Governing Equations of Motion based on MCST

Using Hamilton's principle, the equations of motions can be derived from

$$\delta H = \delta \int_{t_1}^{t_2} (\Pi_k - \Pi_s + \Pi_w)\, dt = 0 \tag{12}$$

where $\delta\Pi_k, \delta\Pi_s$ and $\delta\Pi_w$ indicate the first variation of the kinetic energy, the strain energy and the work done by the external forces, respectively.

The kinetic energy, Π_k, is defined as

$$\Pi_k = \frac{1}{2}\rho \int_0^L \int_A \left((\frac{\partial u_1}{\partial t})^2 + (\frac{\partial u_2}{\partial t})^2 + (\frac{\partial u_3}{\partial t})^2 \right) dA dx =$$

$$\frac{1}{2}\int_0^L \begin{bmatrix} m_0 (\frac{\partial u}{\partial t})^2 + m_2 (\frac{\partial \varphi}{\partial t})^2 + c_1^2 m_6 (\frac{\partial \varphi}{\partial t} + \frac{\partial^2 w}{\partial x \partial t})^2 + 2m_1 (\frac{\partial u}{\partial t})(\frac{\partial \varphi}{\partial t}) - \\ 2c_1 m_3 (\frac{\partial u}{\partial t})(\frac{\partial \varphi}{\partial t} + \frac{\partial^2 w}{\partial x \partial t}) - 2c_1 m_4 (\frac{\partial \varphi}{\partial t})(\frac{\partial \varphi}{\partial t} + \frac{\partial^2 w}{\partial x \partial t}) + m_0 (\frac{\partial w}{\partial t})^2 \end{bmatrix} dx \tag{13}$$

Thus, the first variation of Π_k, Π_s and Π_w gives

$$\delta\Pi_k =$$

$$\int_0^L \begin{bmatrix} \left(-m_0 \frac{\partial^2 u}{\partial t^2} - \bar{m}_1 \frac{\partial^2 \varphi}{\partial t^2} + c_1 m_3 \frac{\partial^3 w}{\partial x \partial t^2} \right) \delta u - \left(\bar{m}_1 \frac{\partial^2 u}{\partial t^2} + \widehat{m}_2 \frac{\partial^2 \varphi}{\partial t^2} - c_1 \bar{m}_4 \frac{\partial^3 w}{\partial x \partial t^2} \right) \delta\varphi - \\ \left(m_0 \frac{\partial^2 w}{\partial t^2} + c_1 m_3 \frac{\partial^3 u}{\partial x \partial t^2} + c_1 \bar{m}_4 \frac{\partial^3 \varphi}{\partial x \partial t^2} - c_1^2 m_6 \frac{\partial^4 w}{\partial x^2 \partial t^2} \right) \delta w \end{bmatrix} dx \tag{14}$$

where

$$m_i = \int_A \rho z^i dA \tag{15-a}$$

$$\bar{m}_i = m_i - c_1 m_{i+2} = \rho \bar{I}_i; \widehat{m}_i = \bar{m}_i - c_1 \bar{m}_{i+2} = \rho \hat{I}_i \tag{15-b}$$

and $i = 1,2,3$. Also,

$$\delta\Pi_s = \int_0^L \left[\begin{array}{l} \left(-\frac{\partial M_{xx}^{(0)}}{\partial x} \right) \delta u - \left(\frac{\partial \bar{M}_{xx}^{(1)}}{\partial x} - \bar{\bar{Q}}_{xz}^{(0)} + \frac{\partial \bar{\bar{Y}}_{yx}^{(0)}}{\partial x} + c_2 Y_{yz}^{(1)} \right) \delta\varphi - \\ \left(c_1 \frac{\partial^2 M_{xx}^{(3)}}{\partial x^2} + \frac{\partial \bar{\bar{Q}}_{xz}^{(0)}}{\partial x} + \frac{\partial^2 \bar{Y}_{yx}^{(0)}}{\partial x^2} - c_2 \frac{\partial Y_{yz}^{(1)}}{\partial x} \right) \delta w \end{array} \right] dx \quad (16)$$

where

$$\bar{M}_{xx}^{(1)} = M_{xx}^{(1)} - c_1 M_{xx}^{(3)}; \bar{\bar{Q}}_{xz}^{(0)} = Q_{xz}^{(0)} - c_2 Q_{xz}^{(2)} \quad (17\text{-a})$$

$$\bar{\bar{Y}}_{yx}^{(0)} = \frac{1}{2}\left(Y_{yx}^{(0)} - c_2 Y_{yx}^{(2)} \right); \bar{Y}_{yx}^{(0)} = \frac{1}{2}\left(Y_{yx}^{(0)} + c_2 Y_{yx}^{(2)} \right) \quad (17\text{-b})$$

The external work is,

$$\delta\Pi_w = -\int_0^L \left[\left(-\frac{\partial}{\partial x}\left(N_T \frac{\partial w}{\partial x} \right) + q - K_w w - K_d \frac{\partial w}{\partial t} + K_p \frac{\partial^2 w}{\partial x^2} + \frac{\partial}{\partial x}\left(T(x) \frac{\partial w}{\partial x} \right) \right) \delta w + f \delta u \right] dx \quad (18)$$

and $N_T = \int_A (E\alpha\, \Delta T) dA$ is the applied axial thermal force. q and f are the transverse and longitudinal distributed forces. K_w, K_d, K_p are the Winkler, Pasternak and damping coefficients due to the elastic foundation, respectively. $T(x)$ is the axial force due to centrifugal stiffening from the rotation of the nano-beam and is given by [9]

$$T(x) = b \int_x^L \int_{-h/2}^{h/2} \rho \tilde{\omega}^2 x dz dx \quad (19)$$

where $\tilde{\omega}$ is the rotation speed of the nano-beam.

The equations of motion can be derived by substituting the Eqs. (14), (16) and (18) into Eq. (12) based on MCST, and this yields

$$\delta u: -m_0 \frac{\partial^2 u}{\partial t^2} - \bar{m}_1 \frac{\partial^2 \varphi}{\partial t^2} + c_1 m_3 \frac{\partial^3 w}{\partial x \partial t^2} + \frac{\partial M_{xx}^{(0)}}{\partial x} + f = 0 \quad (20\text{-a})$$

$$\delta\varphi: -\bar{m}_1 \frac{\partial^2 u}{\partial t^2} - \hat{m}_2 \frac{\partial^2 \varphi}{\partial t^2} + c_1 \bar{m}_4 \frac{\partial^3 w}{\partial x \partial t^2} + \frac{\partial \bar{M}_{xx}^{(1)}}{\partial x} - \bar{\bar{Q}}_{xz}^{(0)} + \frac{\partial \bar{\bar{Y}}_{yx}^{(0)}}{\partial x} + c_2 Y_{yz}^{(1)} = 0 \quad (20\text{-b})$$

$$\delta w: -m_0 \frac{\partial^2 w}{\partial t^2} - c_1 m_3 \frac{\partial^3 u}{\partial x \partial t^2} - c_1 \bar{m}_4 \frac{\partial^3 \varphi}{\partial x \partial t^2} + c_1^2 m_6 \frac{\partial^4 w}{\partial x^2 \partial t^2} + c_1 \frac{\partial^2 M_{xx}^{(3)}}{\partial x^2} + \frac{\partial \bar{\bar{Q}}_{xz}^{(0)}}{\partial x} + \frac{\partial^2 \bar{Y}_{yx}^{(0)}}{\partial x^2} -$$

$$c_2\frac{\partial Y_{yz}^{(1)}}{\partial x}-\frac{\partial}{\partial x}\left(N_T\frac{\partial w}{\partial x}\right)+q-k_w w-k_d\frac{\partial w}{\partial t}+k_p\frac{\partial^2 w}{\partial x^2}+\frac{\partial}{\partial x}\left(T(x)\frac{\partial w}{\partial x}\right)=0 \tag{20-c}$$

The general boundary conditions are given by

$$\begin{aligned}
&\delta u: && \left[M_{xx}^{(0)}=N_{ex}\right] && \text{or} && [u=\bar{u} \ \text{ at } \ x=0 \ \text{ and } \ x=L]\\
&\delta\varphi: && \left[\bar{M}_{xx}^{(1)}-\frac{1}{2}\bar{\bar{Y}}_{yx}^{(0)}=M_{ex}\right] && \text{or} && [\varphi=\bar{\varphi} \ \text{ at } \ x=0 \ \text{ and } \ x=L]\\
&\delta w: && \left[c_1\bar{m}_4\frac{\partial^2\varphi}{\partial t^2}-c_1^2 m_6\frac{\partial^3 w}{\partial x\partial t^2}+c_1\frac{\partial M_{xx}^{(3)}}{\partial x}+\frac{1}{2}\frac{\partial\bar{Y}_{yx}^{(0)}}{\partial x}+\bar{\bar{Q}}_{xz}^{(0)}-c_2 Y_{yz}^{(1)}\right.\\
& && \left.=V_{ex}\right] && \text{or} && [w=\bar{w} \ \text{ at } \ x=0 \ \text{ and } \ x=L]\\
&\partial\left(\frac{\partial w}{\partial x}\right): && \left[c_1 M_{xx}^{(3)}+\frac{1}{2}\bar{Y}_{yx}^{(0)}=Y_{ex}\right] && \text{or} && \left[\frac{\partial w}{\partial x}=\frac{\partial\bar{w}}{\partial x} \ \text{ at } \ x=0 \ \text{ and } \ x=L\right]
\end{aligned} \tag{21}$$

Here, N_{ex}, V_{ex} are the applied axial and transverse shear forces respectively. Also, M_{ex}, Y_{ex} are applied first- and third-order bending moments at the ends of nano-beam.

Substituting Eqs. (8), (9) and (11) into Eqs. (21), the governing equations of motion are obtained in the terms of displacement. Furthermore, it is easy to show $\bar{m}_1=m_3=0$. Thus

$$\delta u: \ -m_0\frac{\partial^2 u}{\partial t^2}+EI_0\frac{\partial^2 u}{\partial x^2}+f= \tag{22-a}$$

$$\begin{aligned}
&\delta\varphi: \ \ \hat{m}_2\frac{\partial^2\varphi}{\partial t^2}-c_1\bar{m}_4\frac{\partial^3 w}{\partial x\partial t^2}+[G\tilde{I}_0+c_2^2 G l_m^2 I_2]\varphi-\left[E\hat{I}_2-\tfrac{1}{4}G l_m^2 I_0^{'}\right]\frac{\partial^2\varphi}{\partial x^2}+\\
&[\mu\tilde{I}_0+c_2^2 G l_m^2 I_2]\frac{\partial w}{\partial x}+\left[c_1 E\bar{I}_4+\tfrac{1}{4}G l_m^2 I_0^{*}\right]\frac{\partial^3 w}{\partial x^3}=0
\end{aligned} \tag{22-b}$$

$$\begin{aligned}
\delta w: \ &-c_1\bar{m}_4\frac{\partial^3\varphi}{\partial x\partial t^2}-m_0\frac{\partial^2 w}{\partial t^2}+c_1^2 m_6\frac{\partial^4 w}{\partial x^2\partial t^2}-K_d\frac{\partial w}{\partial t}+[G\tilde{I}_0+c_2^2 G l_m^2 I_2]\frac{\partial\varphi}{\partial x}\\
&+\left[c_1 E\bar{I}_4+\frac{1}{4}G l_m^2 I_0^{*}\right]\frac{\partial^3\varphi}{\partial x^3}-K_w w+\left(\frac{\partial T}{\partial x}\right)\frac{\partial w}{\partial x}\\
&+\left[G\tilde{I}_0+c_2^2 G l_m^2 I_2+K_p-N_T+T\right]\frac{\partial^2 w}{\partial x^2}-\left[c_1^2 E I_6+\frac{1}{4}G l_m^2 I_0^{''}\right]\frac{\partial^4 w}{\partial x^4}+q\\
&=0
\end{aligned} \tag{22-c}$$

Here, E is Young's modulus and the other parameters are defined as

$$\begin{aligned}
&I_i=\int_A z^i dA\\
&\bar{I}_i=I_i-c_1 I_{i+2}; \quad \hat{I}_i=\bar{I}_i-c_1\bar{I}_{i+2}\\
&\bar{\bar{I}}_i=I_i+c_2 I_{i+2}; \quad \tilde{I}_i=\bar{I}_i-c_2\bar{I}_{i+2}; \quad I_i^{*}=I_i-c_2 I_{i+2}
\end{aligned} \tag{23}$$

$I_i^{'} = I_i^* - c_2 I_{i+2}^*; \quad I_i^{''} = \bar{\bar{I}}_i + c_2 \bar{\bar{I}}_{i+2}$
$\underset{\sim}{I}_i = I_i^* + c_2 I_{i+2}^* = \bar{\bar{I}}_i - c_2 \bar{\bar{I}}_{i+2}$
for $i = 0, \ldots, 6$.

2.3. Eringen's Nonlocal Theory (ENT)

According to Eringen's nonlocal theory [14], the stress field at any point $\boldsymbol{x}$ is a function of both the strain field corresponding to that point (the hyper-elastic case) and all other strain fields of the configuration. Hence, the nonlocal stress tensor is calculated as

$$\boldsymbol{\sigma} = \int_V \kappa(|\boldsymbol{x}' - \boldsymbol{x}|, \eta)\boldsymbol{t}(\boldsymbol{x}')d\boldsymbol{x}' \tag{24}$$

where $\boldsymbol{t}(.)$ denotes the local stress tensor at point $(.)$ and $\kappa(|\boldsymbol{x}' - \boldsymbol{x}|, \eta)$ is the nonlocal modulus. Thus, the general from of the nonlocal characteristics may be represented by the differential form as [14]

$$[1 - (e_0 a)^2 \nabla^2] t_{ij} = \lambda \varepsilon_{rr} \delta_{ij} + \mu \varepsilon_{ij} \tag{25}$$

where t_{ij} and ε denote the nonlocal stress and strain tensor, respectively and $e_0 a$ is the nonlocal parameter and $\nabla^2 = \frac{\partial^2}{\partial x^2}$. Therefore, the nonlocal constitutive relations are given as

$$\sigma_{xx} - (e_0 a)^2 \frac{\partial^2 \sigma_{xx}}{\partial x^2} = E \varepsilon_{xx} \tag{26-a}$$

$$\sigma_{xz} - (e_0 a)^2 \frac{\partial^2 \sigma_{xz}}{\partial x^2} = 2\mu \varepsilon_{xz} \tag{26-b}$$

Using Eqs. (11-a) and (17-a), the nonlocal constitutive relations in Eqs. (26) can be developed as

$$M_{xx}^{(0)} - (e_0 a)^2 \frac{\partial^2 M_{xx}^{(0)}}{\partial x^2} = E I_0 \frac{\partial u}{\partial x} \tag{27-a}$$

$$\bar{M}_{xx}^{(1)} - (e_0 a)^2 \frac{\partial^2 \bar{M}_{xx}^{(1)}}{\partial x^2} = E \bar{I}_2 \frac{\partial \varphi}{\partial x} - c_1 E \bar{I}_4 \left(\frac{\partial \varphi}{\partial x} + \frac{\partial^2 w}{\partial x^2}\right) \tag{27-b}$$

$$M_{xx}^{(3)} - (e_0 a)^2 \frac{\partial^2 M_{xx}^{(3)}}{\partial x^2} = E I_4 \frac{\partial \varphi}{\partial x} - c_1 E I_6 \left(\frac{\partial \varphi}{\partial x} + \frac{\partial^2 w}{\partial x^2}\right) \tag{27-c}$$

$$\bar{\bar{Q}}_{xz}^{(0)} - (e_0a)^2 \frac{\partial^2 \bar{\bar{Q}}_{xz}^{(0)}}{\partial x^2} = G\tilde{I}_0(\varphi + \frac{\partial w}{\partial x}) \tag{27-d}$$

Again, Hamilton's principle for third-order beam theory is employed to extract the governing equations of motion based on Eringen's nonlocal theory. Here, the kinetic energy and external work done are identical to MCST and only the strain energy density, Π_s, is different and described by

$$\Pi_s = \int_0^L \left[M_{xx}^{(0)} \frac{\partial u}{\partial x} + M_{xx}^{(1)} \frac{\partial \varphi}{\partial x} - c_1 M_{xx}^{(3)} (\frac{\partial \varphi}{\partial x} + \frac{\partial^2 w}{\partial x^2}) + Q_{xz}^{(0)} (\varphi + \frac{\partial w}{\partial x}) - c_2 Q_{xz}^{(2)} (\varphi + \frac{\partial w}{\partial x}) \right] dx \tag{28}$$

The variation is then

$$\delta\Pi_s = \int_0^L \left[\left(-\frac{\partial M_{xx}^{(0)}}{\partial x} \right) \delta u - \left(\frac{\partial \bar{M}_{xx}^{(1)}}{\partial x} - \bar{\bar{Q}}_{xz}^{(0)} \right) \delta\varphi - \left(c_1 \frac{\partial^2 M_{xx}^{(3)}}{\partial x^2} + \frac{\partial \bar{\bar{Q}}_{xz}^{(0)}}{\partial x} \right) \delta w \right] dx \tag{29}$$

Therefore, substituting Eqs. (14), (18) and (29) into Eq. (12), employing Eq. (27) and applying some algebraic simplifications results in the governing equations of motion based on Eringen's nonlocal theory as

$$\delta u: \quad -m_0 \left[\frac{\partial^2 u}{\partial t^2} - (e_0a)^2 \frac{\partial^4 u}{\partial x^2 \partial t^2} \right] + \left[f - (e_0a)^2 \frac{\partial^2 f}{\partial x^2} \right] + EI_0 \frac{\partial^2 u}{\partial x^2} = 0 \tag{30-a}$$

$$\delta\varphi: \quad \hat{m}_2 \left[\frac{\partial^2 \varphi}{\partial t^2} - (e_0a)^2 \frac{\partial^4 \varphi}{\partial x^2 \partial t^2} \right] - c_1 \bar{m}_4 \left[\frac{\partial^3 w}{\partial x \partial t^2} - (e_0a)^2 \frac{\partial^5 w}{\partial x^3 \partial t^2} \right] + G\tilde{I}_0 \varphi - E\hat{I}_2 \frac{\partial^2 \varphi}{\partial x^2} + G\tilde{I}_0 \frac{\partial w}{\partial x} + c_1 E\bar{I}_4 \frac{\partial^3 w}{\partial x^3} = 0 \tag{30-b}$$

$$\delta w: \quad -c_1 \bar{m}_4 \left[\frac{\partial^3 \varphi}{\partial x \partial t^2} - (e_0a)^2 \frac{\partial^5 \varphi}{\partial x^3 \partial t^2} \right] - \left[m_0 \frac{\partial^2 w}{\partial t^2} - (c_1^2 m_6 + (e_0a)^2 m_0) \frac{\partial^4 w}{\partial x^2 \partial t^2} + (e_0a)^2 c_1^2 m_6 \frac{\partial^6 w}{\partial x^4 \partial t^2} \right] - K_d \left[\frac{\partial w}{\partial t} - (e_0a)^2 \frac{\partial^3 w}{\partial x^2 \partial t} \right] + G\tilde{I}_0 \frac{\partial \varphi}{\partial x} + c_1 E\bar{I}_4 \frac{\partial^3 \varphi}{\partial x^3} - K_w w + \left[\frac{\partial T}{\partial x} - (e_0a)^2 \frac{\partial^3 T}{\partial x^3} \right] \frac{\partial w}{\partial x} + \left[G\tilde{I}_0 + K_p + (e_0a)^2 K_w - N_T + T - 3(e_0a)^2 \frac{\partial^2 T}{\partial x^2} \right] \frac{\partial^2 w}{\partial x^2} - \left[3(e_0a)^2 \frac{\partial T}{\partial x} \right] \frac{\partial^3 w}{\partial x^3} -$$

$$\left[c_1^2 EI_6 + (e_0a)^2 K_p + (e_0a)^2 T - (e_0a)^2 N_T\right]\frac{\partial^4 w}{\partial x^4} + q - (e_0a)^2\frac{\partial^2 q}{\partial x^2} = 0 \qquad (30\text{-c})$$

The general boundary conditions are given by

$$\delta u: \quad \left[M_{xx}^{(0)} + m_0(e_0a)^2\frac{\partial^3 u}{\partial x \partial t^2} = N_{ex}\right] \quad \text{or} \quad [u = \bar{u} \ \text{ at } \ x = 0 \ \text{ and } \ x = L]$$

$$\delta\varphi: \quad \left[\bar{M}_{xx}^{(1)} + (e_0a)^2\left(\hat{m}_2\frac{\partial^3\varphi}{\partial x\partial t^2} - c_1\bar{m}_4\frac{\partial^4 w}{\partial x^2\partial t^2} - c_1\frac{\partial^2 M_{xx}^{(3)}}{\partial x^2}\right) = M_{ex}\right] \quad \text{or} \quad [\varphi = \bar{\varphi} \ \text{ at } \ x = 0 \ \text{ and } \ x = L]$$

$$\delta w: \quad \left[c_1\bar{m}_4\frac{\partial^2\varphi}{\partial t^2} - c_1^2 m_6\frac{\partial^3 w}{\partial x\partial t^2} + c_1\frac{\partial M_{xx}^{(3)}}{\partial x} + \bar{\bar{Q}}_{xz}^{(0)} + \frac{\partial}{\partial x}(e_0a)^2\left(-c_1\frac{\partial^2 M_{xx}^{(3)}}{\partial t^2} + c_1\bar{m}_4\frac{\partial^3\varphi}{\partial x\partial t^2} + m_0\frac{\partial^2 w}{\partial t^2} - c_1^2 m_6\frac{\partial^4 w}{\partial x^2\partial t^2}\right) = V_{ex}\right] \quad \text{or} \quad [w = \bar{w} \ \text{ at } \ x = 0 \ \text{ and } \ x = L]$$

$$\partial\left(\frac{\partial w}{\partial x}\right): \quad \left[c_1 M_{xx}^{(3)} = Y_{ex}\right] \quad \text{or} \quad \left[\frac{\partial w}{\partial x} = \frac{\partial\bar{w}}{\partial x} \ \text{ at } \ x = 0 \ \text{ and } \ x = L\right] \qquad (31)$$

2.4. Dimensionless Governing Equations Based on MCST and ENT

Eqs. (22) and (30) are the equations of motions in terms of the generalized displacements based on MCST and ENT respectively. The equations have been derived by considering the effects of the viscoelastic foundation, thermal forces and the centrifugal stiffening due to the rotation of the nano-beam. To establish the dimensionless equations of motion, the dimensionless parameters are introduced as

$$\begin{aligned}
&\zeta = \frac{x}{L}; W = \frac{w}{L}; \Phi = \varphi; \mu = \frac{e_0a}{L}; l_0 = \frac{l_m}{h}\\
&\bar{\tau} = \frac{T}{T_{max}}; \bar{q} = \frac{qL}{EI_0}; \bar{f} = \frac{fL}{EI_0}; \vartheta = \frac{N_T}{EI_0}; \Omega^2 = \frac{m_2\omega^2}{EI_0}\\
&\bar{M}_0 = \frac{m_0L^2}{m_2}; \bar{M}_1 = \frac{\bar{m}_1L}{m_2}; \bar{M}_2 = \frac{\hat{m}_2}{m_2}; \bar{M}_3 = \frac{c_1m_3L}{m_2}; \bar{M}_4 = \frac{c_1\bar{m}_4}{m_2}; \bar{M}_6 = \frac{c_1^2m_6}{m_2}\\
&\alpha_0 = \frac{G\tilde{I}_0}{EI_0}; \alpha_2 = \frac{E\hat{I}_2}{EI_0L^2}; \alpha_4 = \frac{c_1E\bar{I}_4}{EI_0L^2}; \alpha_6 = \frac{c_1^2EI_6}{EI_0L^2}\\
&\beta_0^{'} = \frac{Gl_m^2I_0^{'}}{4EI_0L^2}; \beta_0^{''} = \frac{Gl_m^2I_0^{''}}{4EI_0L^2}; \underset{\sim}{\beta}_0 = \frac{Gl_m^2I_0}{4EI_0L^2}; \beta_2 = \frac{G_2^2\mu l_m^2I_2}{EI_0}
\end{aligned} \qquad (32)$$

$k_d = \frac{K_d L^2}{\sqrt{EI_0 m_2}}; k_w = \frac{K_w L^2}{EI_0}; k_p = \frac{K_p}{EI_0}; \Im = \frac{T_{max}}{EI_0}$

where

$T_{max} = \frac{1}{2} m_0 L^2 \widetilde{\omega}^2$ (33)

Substituting Eq. (32) into Eqs. (22) and (30) yields the non-dimensional governing equations of motions in terms of rotation and displacements for MCST and ENT as:

1- MCST:

$$-\bar{M}_0 \frac{\partial^2 U}{\partial t^2} + \frac{\partial^2 U}{\partial \zeta^2} + \bar{f} = 0 \quad (34\text{-a})$$

$$\left[\bar{M}_2 \frac{\partial^2 \Phi}{\partial t^2} - \bar{M}_4 \frac{\partial^3 W}{\partial \zeta \partial t^2}\right] + [\alpha_0 + \beta_2]\Phi - \left[\alpha_2 + \beta_0^{'}\right] \frac{\partial^2 \Phi}{\partial \zeta^2} + [\alpha_0 + \beta_2] \frac{\partial W}{\partial \zeta} + \left[\alpha_4 + \underset{\sim}{\beta_0}\right] \frac{\partial^3 W}{\partial \zeta^3} = 0 \quad (34\text{-b})$$

$$\left[-\bar{M}_4 \frac{\partial^3 \Phi}{\partial \zeta \partial t^2} - \bar{M}_0 \frac{\partial^2 W}{\partial t^2} + \bar{M}_6 \frac{\partial^4 W}{\partial \zeta^2 \partial t^2}\right] - k_d \frac{\partial W}{\partial t} + [\alpha_0 + \beta_2] \frac{\partial \Phi}{\partial \zeta} + \left[\alpha_4 + \underset{\sim}{\beta_0}\right] \frac{\partial^3 \Phi}{\partial \zeta^3} - k_w W + \Im \left[\frac{\partial \bar{\tau}}{\partial \zeta}\right] \frac{\partial W}{\partial \zeta} + \left[\Im \bar{\tau} + \alpha_0 + \beta_2 + k_p - \vartheta\right] \frac{\partial^2 W}{\partial \zeta^2} - \left[\alpha_6 + \beta_0^{''}\right] \frac{\partial^4 W}{\partial \zeta^4} + \bar{q} = 0 \quad (34\text{-c})$$

2- ENT:

$$-\bar{M}_0 \frac{\partial^2 U}{\partial t^2} + \mu^2 \bar{M}_0 \frac{\partial^4 U}{\partial \zeta^2 \partial t^2} + \frac{\partial^2 U}{\partial \zeta^2} + \bar{f} - \mu^2 \frac{\partial^2 \bar{f}}{\partial \zeta^2} = 0 \quad (35\text{-a})$$

$$\left[\bar{M}_2 \frac{\partial^2 \Phi}{\partial t^2} - \mu^2 \bar{M}_2 \frac{\partial^4 \Phi}{\partial \zeta^2 \partial t^2} - \bar{M}_4 \frac{\partial^3 W}{\partial \zeta \partial t^2} + \mu^2 \bar{M}_4 \frac{\partial^5 W}{\partial \zeta^3 \partial t^2}\right] + \alpha_0 \Phi - \alpha_2 \frac{\partial^2 \Phi}{\partial \zeta^2} + \alpha_0 \frac{\partial W}{\partial \zeta} + \alpha_4 \frac{\partial^3 W}{\partial \zeta^3} = 0 \quad (35\text{-b})$$

$$\left[-\bar{M}_4 \frac{\partial^3 \Phi}{\partial \zeta \partial t^2} + \mu^2 \bar{M}_4 \frac{\partial^5 \Phi}{\partial \zeta^3 \partial t^2} - \bar{M}_0 \frac{\partial^2 W}{\partial t^2} + (\bar{M}_6 + \mu^2 \bar{M}_0) \frac{\partial^4 W}{\partial \zeta^2 \partial t^2} - \mu^2 \bar{M}_6 \frac{\partial^6 W}{\partial \zeta^4 \partial t^2}\right] + \left[-k_d \frac{\partial W}{\partial t} + \mu^2 k_d \frac{\partial^3 W}{\partial \zeta^2 \partial t}\right] + \alpha_0 \frac{\partial \Phi}{\partial \zeta} + \alpha_4 \frac{\partial^3 \Phi}{\partial \zeta^3} - k_w W + \Im \left[\frac{\partial \bar{\tau}}{\partial \zeta} - \mu^2 \frac{\partial^3 \bar{\tau}}{\partial \zeta^3}\right] \frac{\partial W}{\partial \zeta} + \left[\Im \bar{\tau} - 3\mu^2 \Im \frac{\partial^2 \bar{\tau}}{\partial \zeta^2} + \alpha_0 + k_p + \mu^2 k_w - \vartheta\right] \frac{\partial^2 W}{\partial \zeta^2} - \left[3\mu^2 \Im \frac{\partial \bar{\tau}}{\partial \zeta}\right] \frac{\partial^3 W}{\partial \zeta^3} - \left[-\mu^2 \Im \bar{\tau} + \alpha_6 + \mu^2 k_p - \mu^2 \vartheta\right] \frac{\partial^4 W}{\partial \zeta^4} + \bar{q} - \mu^2 \frac{\partial^2 \bar{q}}{\partial \zeta^2} = 0 \quad (35\text{-c})$$

3. Solution Procedure

3.1 Generalized Differential Quadrature Method

The GDQM is an efficient and robust numerical solution technique, and hence is adopted to solve the equations of motion of the rotating nanobeam and calculate the results. Based on the GDQM, the domain of the nanobeam is discretized into N_x mesh points in the x direction. The mesh points are generated by the Chebyshev–Gauss–Lobatto distribution as

$$x_i = \frac{1}{2}\left(1 - \cos\left(\frac{i-1}{N_x-1}\pi\right)\right) \qquad i = 1, \ldots, N_x \tag{36}$$

To implement the GDQM, all of the derivatives of $f(x)$ at each mesh point x_i are defined via a linear weighted sum as

$$\frac{\partial^n f(x)}{\partial x^n}|(x_i) = \sum_{k=1}^{N_x} \Lambda_{ik}^{x(n)} f(x_k) \tag{37}$$

where $i = 1, .., N_x$ and $\Gamma_{ik}^{x(n)}$ are weighting coefficients corresponding to the n^{th} order derivative with respect to x. The weighting coefficients for the first order derivative are

$$\Lambda_{ik}^{(1)} = \begin{cases} \frac{\Gamma(x_i)}{(x_i - x_k)\Gamma(x_k)} & \text{for} \quad i \neq k \\ -\sum_{\substack{k=1 \\ i \neq k}}^{N_x} \Lambda_{ik}^{(1)} & \text{for} \quad i = k \end{cases} \tag{38}$$

where $\Gamma(x_i)$ are the Lagrangian polynomials given by

$$\Gamma(x_i) = \prod_{\substack{k=1 \\ i \neq k}}^{N_x} (x_i - x_k) \tag{39}$$

The weighting coefficients for the higher order derivatives may be calculated as [65]

$$\Lambda_{ik}^{(n)} = \sum_{p=1}^{N_x} \Lambda_{ip}^{(n-1)} \Lambda_{pk}^{(1)} \qquad n \geq 2 \tag{40}$$

The solution of the equations of motion are assumed to be of the form

$$U(x,t) = \bar{U}(x)\exp(\Omega t)$$
$$W(x,t) = \bar{W}(x)\exp(\Omega t) \tag{41}$$
$$\Phi(x,t) = \bar{\Phi}(x)\exp(\Omega t)$$

where Ω is the dimensionless complex eigenvalue. Using GDQM principles, the governing equations of motion (Eqs. (34) and (35)) for both MCST and ENT are discretized to give

- MCST:

$$\Omega^2[-\bar{M}_0\bar{U}_i] + \sum_{k=1}^{N_x} \Lambda_{ik}^{(2)}\bar{U}_k + \bar{f} = 0 \tag{42-a}$$

$$\Omega^2\left[\bar{M}_2\bar{\Phi}_i - \bar{M}_4\sum_{k=1}^{N_x}\Lambda_{ik}^{(1)}\bar{W}_k\right] + [\alpha_0+\beta_2]\bar{\Phi}_i - \left[\alpha_2+\beta_0'\right]\sum_{k=1}^{N_x}\Lambda_{ik}^{(2)}\bar{\Phi}_k +$$
$$[\alpha_0+\beta_2]\sum_{k=1}^{N_x}\Lambda_{ik}^{(1)}\bar{W}_k + \left[\alpha_4+\underset{\sim}{\beta_0}\right]\sum_{k=1}^{N_x}\Lambda_{ik}^{(3)}\bar{W}_k = 0 \tag{42-b}$$

$$\Omega^2[-\bar{M}_4\sum_{k=1}^{N_x}\Lambda_{ik}^{(1)}\bar{\Phi}_k - \bar{M}_0\bar{W}_i + \bar{M}_6\sum_{k=1}^{N_x}\Lambda_{ik}^{(2)}\bar{W}_k] + \Omega[-k_d\bar{W}_i] + [\alpha_0+\beta_2]\sum_{k=1}^{N_x}\Lambda_{ik}^{(1)}\bar{\Phi}_k +$$
$$\left[\alpha_4+\underset{\sim}{\beta_0}\right]\sum_{k=1}^{N_x}\Lambda_{ik}^{(3)}\bar{\Phi}_k - k_w\bar{W}_i + \Im\sum_{k=1}^{N_x}\Lambda_{ik}^{(1)}\bar{\tau}_k\sum_{k=1}^{N_x}\Lambda_{ik}^{(1)}\bar{W}_k + \left[\Im\bar{\tau}_i + \alpha_0 + \beta_2 + k_p -\right.$$
$$\left.\vartheta\right]\sum_{k=1}^{N_x}\Lambda_{ik}^{(2)}\bar{W}_k - \left[\alpha_6+\beta_{0_i}''\right]\sum_{k=1}^{N_x}\Lambda_{ik}^{(4)}\bar{W}_k + \bar{q} = 0 \tag{42-c}$$

- ENT:

$$\Omega^2\left[-\bar{M}_0\bar{U}_i + \mu^2\bar{M}_0\sum_{k=1}^{N_x}\Lambda_{ik}^{(2)}\bar{U}_k\right] + \sum_{k=1}^{N_x}\Lambda_{ik}^{(2)}\bar{U}_k + \bar{f} - \mu^2\frac{\partial^2\bar{f}}{\partial\zeta^2} = 0 \tag{43-a}$$

$$\Omega^2\left[\bar{M}_2\bar{\Phi}_i - \mu^2\bar{M}_2\sum_{k=1}^{N_x}\Lambda_{ik}^{(2)}\bar{\Phi}_k - \bar{M}_4\sum_{k=1}^{N_x}\Lambda_{ik}^{(1)}\bar{W}_k + \mu^2\bar{M}_4\sum_{k=1}^{N_x}\Lambda_{ik}^{(3)}\bar{W}_k\right] + \alpha_0\bar{\Phi}_i -$$

$$\alpha_2 \sum_{k=1}^{N_x} \Lambda_{ik}^{(2)} \bar{\Phi}_k + \alpha_0 \sum_{k=1}^{N_x} \Lambda_{ik}^{(1)} \bar{W}_k + \alpha_4 \sum_{k=1}^{N_x} \Lambda_{ik}^{(3)} \bar{W}_k = 0 \tag{43-b}$$

$$\Omega^2[-\bar{M}_4 \sum_{k=1}^{N_x} \Lambda_{ik}^{(1)} \bar{\Phi}_k + \mu^2 \bar{M}_4 \sum_{k=1}^{N_x} \Lambda_{ik}^{(3)} \bar{\Phi}_k - \bar{M}_0 \bar{W}_i + (\bar{M}_6 + \mu^2 \bar{M}_0) \sum_{k=1}^{N_x} \Lambda_{ik}^{(2)} \bar{W}_k -$$

$$\mu^2 \bar{M}_6 \sum_{k=1}^{N_x} \Lambda_{ik}^{(4)} \bar{W}_k] + \Omega\left[-k_d \bar{W}_i + \mu^2 k_d \sum_{k=1}^{N_x} \Lambda_{ik}^{(2)} \bar{W}_k\right] + \alpha_0 \sum_{k=1}^{N_x} \Lambda_{ik}^{(1)} \bar{\Phi}_k +$$

$$\alpha_4 \sum_{k=1}^{N_x} \Lambda_{ik}^{(3)} \bar{\Phi}_k - k_w \bar{W}_i + \Im\left[\sum_{k=1}^{N_x} \Lambda_{ik}^{(1)} \bar{\tau}_k - \mu^2 \sum_{k=1}^{N_x} \Lambda_{ik}^{(3)} \bar{\tau}_k\right] \sum_{k=1}^{N_x} \Lambda_{ik}^{(1)} \bar{W}_k +$$

$$\left[\Im \bar{\tau}_i - 3\mu^2 \Im \sum_{k=1}^{N_x} \Lambda_{ik}^{(2)} \bar{\tau}_k + \alpha_0 + k_p + \mu^2 k_w - \vartheta\right] \sum_{k=1}^{N_x} \Lambda_{ik}^{(2)} \bar{W}_k -$$

$$\left[3\mu^2 \Im \sum_{k=1}^{N_x} \Lambda_{ik}^{(1)} \bar{\tau}_k\right] \sum_{k=1}^{N_x} \Lambda_{ik}^{(3)} \bar{W}_k - \left[\alpha_6 + \mu^2 k_p - \mu^2 \vartheta - \mu^2 \Im \bar{\tau}_i\right] \sum_{k=1}^{N_x} \Lambda_{ik}^{(4)} \bar{W}_k + \bar{q} -$$

$$\mu^2 \frac{\partial^2 \tilde{q}}{\partial \zeta^2} = 0 \tag{43-c}$$

where $\bar{U}_i = \bar{U}(x_i)$, $\bar{W}_i = \bar{W}(x_i)$ and $\bar{\Phi}_i = \bar{\Phi}(x_i)$. Equation (42) for MCST and Eq. (43) for ENT can be rewritten as

$$[\mathbf{K} + \Omega \mathbf{C} + \Omega^2 \mathbf{M}]\mathbf{Z} = \mathbf{0} \tag{44}$$

where

$$\bar{\mathbf{Z}} = \begin{Bmatrix} \bar{\mathbf{U}} \\ \bar{\mathbf{W}} \\ \bar{\mathbf{\Phi}} \end{Bmatrix} \tag{45}$$

and $\bar{\mathbf{U}}, \bar{\mathbf{W}}$ and $\bar{\mathbf{\Phi}}$ are vectors whose *i* th elements are $\bar{U}_i$, $\bar{W}_i$ and $\bar{\Phi}_i$, respectively. **M**, **C** and **K** are the equivalent mass, damping and stiffness matrices, which are obtained by arranging the elements from Eqs. (42) for MCST and Eqs. (43) for ENT and have the form

$$\mathbf{M} = \begin{bmatrix} \mathbf{M}_{\bar{U}\bar{U}} & \mathbf{M}_{\bar{U}\bar{W}} & \mathbf{M}_{\bar{U}\bar{\Phi}} \\ \mathbf{M}_{\bar{W}\bar{U}} & \mathbf{M}_{\bar{W}\bar{W}} & \mathbf{M}_{\bar{W}\bar{\Phi}} \\ \mathbf{M}_{\bar{\Phi}\bar{U}} & \mathbf{M}_{\bar{\Phi}\bar{W}} & \mathbf{M}_{\bar{\Phi}\bar{\Phi}} \end{bmatrix}_{3N_x \times 3N_x} \tag{46-a}$$

$$\mathbf{C} = \begin{bmatrix} \mathbf{C}_{\bar{U}\bar{U}} & \mathbf{C}_{\bar{U}\bar{W}} & \mathbf{C}_{\bar{U}\bar{\Phi}} \\ \mathbf{C}_{\bar{W}\bar{U}} & \mathbf{C}_{\bar{W}\bar{W}} & \mathbf{C}_{\bar{W}\bar{\Phi}} \\ \mathbf{C}_{\bar{\Phi}\bar{U}} & \mathbf{C}_{\bar{\Phi}\bar{W}} & \mathbf{C}_{\bar{\Phi}\bar{\Phi}} \end{bmatrix}_{3N_x \times 3N_x} \tag{46-b}$$

$$\mathbf{K} = \begin{bmatrix} \mathbf{K}_{\bar{U}\bar{U}} & \mathbf{K}_{\bar{U}\bar{W}} & \mathbf{K}_{\bar{U}\bar{\Phi}} \\ \mathbf{K}_{\bar{W}\bar{U}} & \mathbf{K}_{\bar{W}\bar{W}} & \mathbf{K}_{\bar{W}\bar{\Phi}} \\ \mathbf{K}_{\bar{\Phi}\bar{U}} & \mathbf{K}_{\bar{\Phi}\bar{W}} & \mathbf{K}_{\bar{\Phi}\bar{\Phi}} \end{bmatrix}_{3N_x \times 3N_x} \tag{46-c}$$

For eigenvalue analysis, Eq. (44) and the boundary conditions should be satisfied simultaneously. Based on DQM, the boundary conditions can be written as constraints on the degrees of freedom as

$$\mathbf{R}^T \bar{\mathbf{Z}} = \mathbf{0} \tag{47}$$

where $\mathbf{R}$ is matrix that depends on the type of boundary conditions. Boundary conditions involving derivatives can be defined in the form of Eq. (47) by using Eq. (38). The boundary conditions can be enforced by defining a transformation $\mathbf{T}$, which is orthogonal to $\mathbf{R}$, i.e. $\mathbf{R}^T\mathbf{T} = \mathbf{0}$, and where the matrix $[\mathbf{R}\ \mathbf{T}]$ is square and non-singular. One convenient option is to choose the correct number of boundary degrees of freedom (i.e. equal to the number of boundary conditions) and reorder $\bar{\mathbf{Z}}$ as $\bar{\mathbf{Z}} = \begin{Bmatrix} \bar{\mathbf{Z}}_b \\ \bar{\mathbf{Z}}_d \end{Bmatrix}$, so that $\mathbf{R}$ becomes

$$\mathbf{R}^T = [\mathbf{R}_b\ \mathbf{R}_d] \tag{48}$$

where $\mathbf{R}_b$ is square and non-singular. A suitable transformation is then

$$\mathbf{T} = \begin{Bmatrix} -\mathbf{R}_b^{-1}\mathbf{R}_d \\ \mathbf{I} \end{Bmatrix}, \tag{49}$$

which eliminates the boundary degrees of freedom since

$$\bar{\mathbf{Z}} = \begin{Bmatrix} \bar{\mathbf{Z}}_b \\ \bar{\mathbf{Z}}_d \end{Bmatrix} = \mathbf{T}\bar{\mathbf{Z}}_d \tag{50}$$

The mass and stiffness matrices are then rearranged to match the ordering given in Eq. (48), and the transformed mass, damping and stiffness matrices are

$$\bar{\mathbf{M}} = \mathbf{T}^T\mathbf{M}\mathbf{T} \text{ and } \bar{\mathbf{C}} = \mathbf{T}^T\mathbf{C}\mathbf{T} \text{ and } \bar{\mathbf{K}} = \mathbf{T}^T\mathbf{K}\mathbf{T} \tag{51}$$

The eigenvalue problem then becomes

$$[\bar{\mathbf{K}} + \Omega\bar{\mathbf{C}} + \Omega^2\bar{\mathbf{M}}]\bar{\mathbf{Z}}_d = \mathbf{0} \tag{52}$$

The standard form for the solution of the eigenvalue problem in Eq. (52) is:

$$\begin{bmatrix} -\bar{\mathbf{M}}^{-1}\mathbf{C} & -\bar{\mathbf{M}}^{-1}\mathbf{K} \\ \mathbf{I} & \mathbf{0} \end{bmatrix} \begin{Bmatrix} \dot{\bar{\mathbf{Z}}}_d \\ \bar{\mathbf{Z}}_d \end{Bmatrix} = \Omega \begin{Bmatrix} \dot{\bar{\mathbf{Z}}}_d \\ \bar{\mathbf{Z}}_d \end{Bmatrix} \tag{53}$$

The eigenvalues of Eq. (53) are complex where the real part describes the damping characteristics and the imaginary part gives the damped natural frequency. The boundary conditions are considered based on Eq. (21) for MCST and Eq. (31) for ENT. For example, if the clamped-clamped boundary condition is considered, then

$$\bar{U}_1 = \bar{\Phi}_1 = \bar{U}_{N_x} = \bar{\Phi}_{N_x} = 0$$

$$\bar{W}_1 = \bar{W}_{N_x} = \bar{W}_1^{'} = \bar{W}_{N_x}^{'} = 0 \tag{54}$$

where $\bar{W}_i^{'} = \frac{\partial \bar{W}_i}{\partial x}$.

Other boundary conditions and their implementation in DQM (i.e. how derivatives may be written as a linear combination of elements of $\bar{\mathbf{Z}}$) are given in detail by Behera and Chakraverty [58].

4. Numerical Results and Discussions

In this section, the numerical results are calculated and discussed for the vibration analysis of a rotating nanobeam in a thermal environment considering the variation of eight

parameters. First, the convergence of DQM is considered in Section 4.1 and then model validation is presented in Section 4.2. The results from section 4.3 to 4.6 are extracted for $k_d = 0$ (non-damped system) and clamped-clamped BCs. The effect of k_d on the frequency and also on the damping ratio are considered in Section 4.7 and discussed in detail. Various BCs and their effects on the fundamental non-dimensional are illustrated in Section 4.8. The effects of the length scale parameter l_m and the nonlocal parameter μ, the non-dimensional Winkler and Pasternak coefficients k_w and k_p, the temperature gradient ΔT, the non-dimensional beam rotating velocity Ω_b and the slenderness ratio $\frac{L}{h}$, the non-dimensional visco-elastic coefficient of foundation k_d and different boundary conditions are shown and discussed in detail. For this purpose, we fix six parameters out of the eight possible parameters in each step and change the remaining two parameters to investigate the effects and their interactions. Only the fundamental natural frequency is given in all cases as an example; if required the effects on higher modes may also be considered. The thermo-mechanical properties of the rotating nanobeam are given in Table 1.

Table 1

4.1. DQM Convergence

Figure 2 shows the convergence of DQM for three first modes based on ENT and MCST for typical parameter values. The rate of convergence of DQM is very fast, and as expected the lower modes converge fastest; accurate results are obtained for the 1st mode with $N \geq 10$ grid points for both ENT and MCST, for the 2nd mode with $N \geq 12$ for MCST and $N \geq 14$ for ENT, and for the 3rd mode with $N \geq 18$ for both ENT and MCST. The convergence for other parameter values has been checked, and sufficient accuracy is obtained in all cases with $N = 31$ grid points for both ENT and MSCT. Hence $N = 31$

is used for all examples in this paper. This demonstrates that accuracy, fast convergence and simplicity are advantages of DQM compared with other numerical methods such as the finite element method, the finite difference method and the boundary element method.

Figure 2

4.2. Model Validation

To validate the current model and verify the accuracy of the model, the numerical results are calculated for the Eringen's nonlocal and the modified couple stress models separately for the material properties given by Ref. [42] and the numerical results compared. The fundamental natural frequency for CC-BCs for two different slenderness ratios, $\frac{L}{h} = 12$ and $\frac{L}{h} = 18$, are given in Table 2. Table 3 presents the fundamental natural frequency for CS and SS boundary conditions with $\frac{L}{h} = 100$. The results given in Tables 2 and 3 show good agreement between the proposed method and that of Ref. [42]. This verifies the accuracy of the proposed model.

Table 2

Table 3

Further verification is employed to demonstrate the accuracy of proposed model. Figure 3(a) compares the results established by ENT with those of Ref. [66] for various BCs. Furthermore, the results extracted by MST are compared to those of Ref. [67] in Fig. 3(b) for SS BCs. All of these comparisons demonstrate the accuracy of the proposed model.

Figure 3

4.3. Effects of Nonlocal and Length-Scale Parameters

The effect of the nondimensional nonlocal parameter μ and the effect the nondimensional length scale parameter L_0 on the non-dimensional fundamental frequency are illustrated in Figs. 3 and 4. The non-dimensional fundamental natural frequency of the rotating nanobeam is shown as a function of the non-dimensional nonlocal parameters and as the non-dimensional length-scale in Fig. 3 and Fig. 4 for different slenderness ratios respectively. From Fig. 3 and based on ENT, due to the decrease in the stiffness of the nanobeam, increasing the non-dimensional nonlocal parameter will reduce the natural frequency. Moreover, for higher values of μ, the slenderness ratio has no significant effect on the nondimensional frequency.

Figure 4

In contrast to ENT, increasing the non-dimensional length-scale parameter will increase the stiffness of the nanobeam and the non-dimensional fundamental frequency for MCST. In addition, for both ENT and MCST, the slope of the frequency becomes steeper as the slenderness ratio increases.

Figure 5

4.4. Effects of Winkler-Pasternak Coefficients

The effects of the Winkler-Pasternak coefficients on the non-dimensional fundamental natural frequency are now considered. The effects of the dimensionless Winkler coefficient, k_w, as μ, L_0 and L/h vary, are shown in Figs. 6 and 7. Figure 6 shows the

variation of the non-dimensional fundamental frequency as a function of k_w for different nonlocal parameter/length scale and slenderness ratios for both ENT (Figs. 6(a) and 6(b)) and MCST (Figs. 6(c) and 6(d)). The fundamental natural frequency increases as the dimensionless Winkler coefficient increases for all slenderness ratios. Moreover, the increasing slenderness ratio and the nonlocal parameter/length scale have a significant effect on the frequency.

Figure 6

Figure 7 shows the variation of the fundamental non-dimensional natural frequency as a function of the Winkler coefficient (Figs. 7(a) and 7(c)) for both ENT and MCST and as a function of the nonlocal parameter (Fig. 7(b)) and length scale (Fig. 7(d)). Clearly, increasing of the Winkler coefficient will increase the fundamental non-dimensional natural frequency. Based on Fig. 7(b), increasing the Winkler coefficient will reduce the effect of the nonlocality.

Figure 7

The effects of the dimensionless Pasternak coefficient k_p are shown in Figs. 8 and 9, where k_p is in the interval 0 to 0.5 in Fig. 8 and 0 to 1.2 in Fig. 9. Figures 8(a) and 8(b) illustrates the fundamental frequency as a function of k_p and the slenderness ratio for ENT, and for $\mu = 0.1$ and $\mu = 0.6$, respectively. For $\mu = 0.1$ and all values of L/h, increasing the Pasternak coefficient will increase the fundamental non-dimensional natural frequency but for higher values of μ (e.g. $\mu = 0.6$) increasing k_p has no effect after certain value (here for $k_p \geq 0.315$). This effect is also observed in Figs. 9(a) and

9(b). The effect of k_p on the fundamental non-dimensional natural frequency for MCST is presented in Figs. 9(c) and 9(d) for $L_0 = 0.1$ and $L_0 = 0.6$, respectively. Thus, it is clear that the fundamental frequency will increase with increasing k_p for all values of slenderness ratio and length scale parameter.

Figure 8

Figure 9

To investigate the effect of k_p on the mode shapes of the nanobeam, the fundamental mode shapes for two distinct values of Pasternak coefficient, namely $k_p = 0.2$ and 0.4, when $\mu = 0.6$ and $\frac{L}{h} = 10$ are plotted in Fig. 10. For $k_p = 0.2$ the mode shape is a first bending mode of a CC beam, whereas for $k_p = 0.4$ the fundamental mode shape has switched to a second bending mode. Hence it is clear that the change in character of the plots in Figs. 8 and 9 occur because of mode switching. For example, when $\mu = 0.6$ and $\frac{L}{h} = 10$ this mode switching occurs for $k_p \geq 0.315$.

Figure 10

4.5. Effects of Temperature

Figure 10 shows the variation of the fundamental non-dimensional natural frequency with temperature for different length scale parameters for MCST. Here, $T_0 = 20°\text{C}$ is assumed as the reference temperature and a uniform temperature gradient is considered. According to Fig. 11, the natural frequency generally decreases with temperature. However, in the range $26 \leq \Delta T \leq 70°\text{C}$ there is a jump in the frequency; the jump temperature depends on the value of length scale parameters, e.g. $\Delta T = 70°\text{C}$ for $L_0 = 0.6$ and $\frac{L}{h} = 100$. This jump is the result of static-instability (critical thermal buckling temperature) of the nano/micro beam that occurs due to the temperature rise in mode 1. The results following the jump point are physically meaningless since the model does not adequately describe

the post-buckling behavior and the variation of temperature should be limited by critical thermal buckling temperature. It is clear that with increasing length scale parameter, the critical thermal buckling temperature will increase and thermal buckling will be delayed.

Figure 11

Figures 12 to 15 show the effects of the temperature variation on the fundamental non-dimensional natural frequency over the temperature interval $0 \leq \Delta T \leq 50°\mathrm{C}$ in different states based on both ENT and MCST. Figure 11 illustrates the fundamental non-dimensional natural frequency as a function of ΔT and size effect parameters. The results based on ENT are presented for two different slenderness ratios, $\frac{L}{h} = 15, 20$, and the nonlocal parameter interval $0 \leq \mu \leq 0.6$ in Figs. 12(a) and 12(b). Also, the same results are plotted for MCST over the length scale parameter interval $0 \leq L_0 \leq 0.6$ in Figs. 12(c) and 12(d). For all situations the fundamental natural frequency decreases with increases in temperature. However, the rate of decrease for ENT is higher than for MSCT. Figure 12(b) also shows that the static-instability will occur for Eringen's nonlocal nanobeam at $\Delta T = 42°\mathrm{C}$ if $\mu = 0.6$ and $\frac{L}{h} = 20$.

Figure 12

Figures 13 and 14 show the fundamental non-dimensional natural frequency as a function of $\Delta T, \mu$ and $\frac{L}{h}$. It is obvious that increasing the temperature gradient reduces the fundamental non-dimensional natural frequency but the slope of the frequency decrease will increase with increasing $\Delta T, \mu$ and $\frac{L}{h}$. The static-instability is visible in Figs. 13(c), 13(d), 14(c) and 14(d). Increasing $\Delta T, \mu$ and $\frac{L}{h}$ will increase the probability of thermal

static-instability.

Figure 13

Figure 14

The fundamental non-dimensional natural frequency as a function of $\Delta T, L_0$ and $\frac{L}{h}$ is also illustrated in Fig. 15. The slope of frequency decrease will be sharper with increasing ΔT and $\frac{L}{h}$ but it will be smoother with increasing L_0. The probability of thermal static-instability for MSCT is less than for ENT.

Figure 15

Figure 16 shows the effect of the temperature gradient on the non-dimensional natural frequency for ENT and MCST for $\frac{L}{h} = 10, 15$. The effect of ΔT for ENT is more significant than for MSCT especially for higher values of nonlocal parameter μ.

Figure 16

4.6. Effects of Beam Rotating Velocity

In this section, the effects of the dimensionless rotating velocity Ω_b of the nanobeam on the natural frequency is considered. The dimensionless beam rotating velocity is defined as

$$\Omega_b = \widetilde{\omega} L^2 \sqrt{\frac{m_0}{EI_2}} \tag{55}$$

where $\widetilde{\omega}, L$ are the rotating velocity and the length of the nanobeam respectively. Figure

16 shows the variation of the non-dimensional fundamental natural frequency with Ω_b for various nonlocal parameters μ based on ENT (Figs. 17(a) and 17(b)) and various length scales L_0 for MCST (Figs. 17(c) and 17(d)). The results are presented for two different slenderness ratios, $\frac{L}{h} = 10, 15$. For MCST, increasing the non-dimensional beam rotating velocity will increase the fundamental non-dimensional natural frequency for all values of L_0 and $\frac{L}{h}$. Also, for higher slenderness ratio the effect of increasing Ω_b will be more significant than the effect of increasing L_0.

For ENT, there are two specific features observable in Figs. 17(a) and 17(b). The first is the existence of a convergence point (CP) at which the frequencies for all nonlocal parameters μ has an identical value. The corresponding rotating velocity is called the convergence velocity Ω_c, and increasing the rotating velocity up to Ω_c has only a mild effect on the natural frequency. In contrast, after passing Ω_c increasing the rotating velocity has a significant effect on the natural frequency. Also, for velocities larger than the convergence rotating velocity, the frequency gradient becomes steeper with increasing nonlocal parameter μ. The second specific feature is the corner rotating velocity Ω_{cor}. Increasing Ω_b up to the corner rotating velocity Ω_{cor} causes an increase in the fundamental natural frequency. However, for higher speeds Ω_b has an insignificant effect on the fundamental natural frequency which seems to be approximately constant. This effect is due to mode switching and the fact that the first bending mode is very sensitive to rotational speed whereas the second bending mode is insensitive. The value of the corner rotating velocity depends on the parameters μ and the slenderness ratio.

Figure 17

For high values of the nonlocal parameter μ, the corner rotating velocity occurs at lower speeds. Also, for large slenderness ratios, the corner rotating velocity is observed at higher

rotating velocities. The change in character of the plots at the corner velocities are again die to mode switching. Comparing ENT and MCST, it is notable that the frequency based on MCST is more affected for high values of Ω_b.

Figure 18

Figures 18 and 19 show the fundamental non-dimensional natural frequency of the rotating nanobeam as a function of μ and $\frac{L}{h}$ and different values of Ω_b based on ENT and MCST. Figure 18 shows that increasing Ω_b affects the nonlocality of the nanobeam in a certain range of μ. This range of μ strongly depends on the value of μ and slenderness ratio. For example, when $\Omega_b = 12$ (Fig. 18(a)) for all values of μ and $\frac{L}{h} \geq 12$ the effect of rotating velocity overcomes the effect of nonlocality and increases the fundamental frequency. However, when $\Omega_b = 60$ (Fig. 18(d)) for all values of slenderness ratio up to a certain value of μ, the effect of rotating velocity overcomes to effect of nonlocality and increases the frequency, but after this value of μ, the effect of nonlocality overcomes the effect of slenderness ratio and causes the frequency to decrease. This phenomenon is due to mode switching.

Figure 19

Figure 19 shows that for MCST, increasing Ω_b will increase the fundamental non-dimensional natural frequency of the rotating nanobeam. However, the rate of increase will reduce as Ω_b increases.

4.7. Effects of Foundation Viscoelastic Damping

The effects of viscoelastic damping on the fundamental non-dimensional damped frequency are now illustrated. Also, the variation of the damping ratio is considered based

on the viscoelastic parameter. Figure 20 show the fundamental non-dimensional damped natural frequency and damping ratio versus the variation of k_d based on the differet values of μ and for ENT. The results are calculated for $\frac{L}{h} = 10$ and k_d is changed from 0 to 18. The fundamental non-dimensional damped frequency decreases when the value of k_d is increased. However, the trend of the damping ratio is the opposite and the damping ratio increases when k_d is increased.

Figure 20

In addition, Figure 21 show the fundamental non-dimensional damped natural frequency and damping ratio versus the variation of k_d for different values of L_0 and for MCST. The fundamental non-dimensional damped frequency and damping ratio decreases and increases respectively when the value of k_d is increased.

Figure 21

The simultaneous effect of the slenderness ratio L/h, the nonlocal parameter μ, length scale parameter L_0 and the non-dimensional viscoelastic coefficient k_d are shown in Fig. 22 for ENT and MCST. Increasing the slenderness ratio above a certain value has no significant effect on the fundamental non-dimensional damped natural frequency or on the damping ratio. Increasing the slenderness ratio up to this value, increases the fundamental non-dimensional damped natural frequency. In contrast the damping ratio decreases.

Figure 22

4.1. Effects of Boundary Conditions

Figure 23 shows the effect of boundary conditions on the fundamental non-dimensional natural frequency for CLS (Classical Theory), ENT ($\mu = 0.05$) and MCST ($L_0 = 0.05$). To obtain the results, three different boundary conditions are considered, namely SS, CS and CC, and the frequency is reported for different slenderness ratios. As expected, the highest frequency is for CC-BCs, the lowest is for SS-BCs, and CS-BCs is in the middle.

Figure 23

Conclusion

The objective of this paper is to present a comprehensive mathematical and mechanical model to investigate the vibration of a rotating nanobeam resting on a visco-elastic Winkler-Pasternak foundation incorporating thermal effects based on the modified couple stress and Eringen's nonlocal elasticity theories. These theories are the most used in the literature due to the inclusion of one additional size dependent length scale parameter. These theories are compared side by side in this study and their impacts/differences on the vibrational behavior are investigated.

A higher order shear deformation beam model was employed to develop the equations of motion and GDQM was utilized to solve the resulting equations. Moreover, the effects of the nonlocal parameter, length scale parameter, the Winkler-Pasternak coefficients, damping ratio, the thermal gradient, the slenderness ratio, the rotating velocity of the viscoelastic nanobeam and also different boundary conditions are simulated and discussed in detail. The notable findings are summarized as:

(1) Based on ENT, increasing the non-dimensional nonlocal parameter will decrease the stiffness of the nanobeam and reduce the natural frequency.

(2) In contrast to ENT, increasing the non-dimensional length-scale parameter will increase the stiffness of the nanobeam and the non-dimensional fundamental frequency for MCST.

(3) The fundamental natural frequency increases as the dimensionless Winkler coefficient increases for all slenderness ratios for both ENT and MCST.

(4) For ENT, increasing the Winkler coefficient will reduce the effect of the nonlocality.

(5) The fundamental natural frequency will increase with increasing Pasternak coefficient for all values of slenderness ratio and length scale parameter for MCST.

(6) For ENT and for higher nonlocal parameter, increasing the Pasternak coefficient has no effect after certain value.

(7) For high values of slenderness ratio, the variation of the nonlocal parameter and length scale parameter has little effect on the oscillations of the system.

(8) The fundamental non-dimensional natural frequency decreases with increasing temperature based on both ENT and MCST.

(9) The probability of thermal static-instability for MSCT is lower than for ENT.

(10) For ENT, increasing the nanobeam rotating velocity up to the corner velocity causes an increase in the fundamental non-dimensional natural frequency. However, increasing Ω_b over Ω_{cor} has no significant effect on the fundamental non-dimensional natural frequency.

(11) For ENT, the values of the corner and convergence rotating velocities depend on the nonlocal parameter and slenderness ratio.

(12) For both ENT and MCST, the fundamental non-dimensional damped frequency and damping ratio decrease and increase respectively when the value of damping is increased.

(13) For ENT, mode switching can take place in some conditions.

Accordingly, due to the significant differences between ENT and MCST illustrated in this study to estimate the behaviour of small-scale structures, it is important to choose the proper theory with the correct size effect parameter. Moreover, MCST cannot be merged with nonlocal theory in a unified model.

Data availability statement

This paper simulates the response of nanobeams using the model that is fully defined in the paper. All of the data required to obtain the results in the paper is available in the tables.

References

[1] J. Yan, L. Tong, C. Li, Y. Zhu, Z. Wang, Exact solutions of bending deflections for nano-beams and nano-plates based on nonlocal elasticity theory, Composite Structures, 125 (2015) 304-313.

[2] A.M. Zenkour, M. Sobhy, A simplified shear and normal deformations nonlocal theory for bending of nanobeams in thermal environment, Physica E: Low-dimensional Systems and Nanostructures, 70 (2015) 121-128.

[3] M.S.A. Houari, A. Bessaim, F. Bernard, A. Tounsi, S. Mahmoud, Buckling analysis of new quasi-3D FG nanobeams based on nonlocal strain gradient elasticity theory and variable length scale parameter, Steel and Composite Structures, 28(1) (2018) 13-24.

[4] B. Karami, D. Shahsavari, S.M.R. Nazemosadat, L. Li, A. Ebrahimi, Thermal buckling of smart porous functionally graded nanobeam rested on Kerr foundation, Steel and Composite Structures, 29(3) (2018) 349-362.

[5] A. Rahmani, S. Faroughi, M. Friswell, The vibration of two-dimensional imperfect functionally graded (2D-FG) porous rotating nanobeams based on general nonlocal theory, Mechanical Systems and Signal Processing, 144 (2020) 106854.

[6] A. Babaei, A. Rahmani, Vibration analysis of rotating thermally-stressed gyroscope, based on modified coupled displacement field method, Mechanics Based Design of Structures and Machines, (2020) 1-10.

[7] R. Ansari, J. Torabi, M. Faghih Shojaei, An efficient numerical method for analyzing the thermal effects on the vibration of embedded single-walled carbon nanotubes based on the nonlocal shell model, Mechanics of Advanced Materials and Structures, 25(6) (2018) 500-511.

[8] F. Ebrahimi, A. Dabbagh, Wave dispersion characteristics of heterogeneous nanoscale beams via a novel porosity-based homogenization scheme, The European Physical Journal Plus, 134(4) (2019) 157.

[9] S. Faroughi, A. Rahmani, M. Friswell, On wave propagation in two-dimensional functionally graded porous rotating nano-beams using a general nonlocal higher-order beam model, Applied Mathematical Modelling, 80 (2020) 169-190.

[10] (!!! INVALID CITATION !!! [11-16]).

[11] R. Ansari, J. Torabi, A. Norouzzadeh, An integral nonlocal model for the free vibration analysis of Mindlin nanoplates using the VDQ method, The European Physical Journal Plus, 135(2) (2020) 206.

[12] A.C. Eringen, Nonlocal polar elastic continua, International journal of engineering science, 10(1) (1972) 1-16.

[13] A.C. Eringen, Linear theory of nonlocal elasticity and dispersion of plane waves, International journal of engineering science, 10(5) (1972) 425-435.

[14] A.C. Eringen, Nonlocal continuum field theories, Springer Science & Business Media, 2002.

[15] M. Shaat, A. Abdelkefi, New insights on the applicability of Eringen's nonlocal theory, International Journal of Mechanical Sciences, 121 (2017) 67-75.

[16] R. Mindlin, H. Tiersten, Effects of couple-stresses in linear elasticity, Archive for Rational Mechanics and Analysis, 11(1) (1962) 415-448.

[17] F. Yang, A. Chong, D.C.C. Lam, P. Tong, Couple stress based strain gradient theory for elasticity, International Journal of Solids and Structures, 39(10) (2002) 2731-2743.

[18] D.C. Lam, F. Yang, A. Chong, J. Wang, P. Tong, Experiments and theory in strain gradient elasticity, Journal of the Mechanics and Physics of Solids, 51(8) (2003) 1477-1508.

[19] J. Torabi, R. Ansari, M. Darvizeh, A C1 continuous hexahedral element for nonlinear vibration analysis of nano-plates with circular cutout based on 3D strain gradient theory, Composite Structures, 205 (2018) 69-85.

[20] R. Augello, E. Carrera, A. Pagani, Unified theory of structures based on micropolar elasticity, Meccanica, 54(11) (2019) 1785-1800.

[21] H. Fei, D. Danhui, C. Wei, Z. Jubao, A novel analysis method for damping characteristic of a type of double-beam systems with viscoelastic layer, Applied Mathematical Modelling, 80 (2020) 911-928.

[22] D. Lisitano, J. Slavič, E. Bonisoli, M. Boltežar, Strain proportional damping in Bernoulli-Euler beam theory, Mechanical Systems and Signal Processing, 145 (2020) 106907.

[23] Y. Lei, S. Adhikari, M. Friswell, Vibration of nonlocal Kelvin–Voigt viscoelastic damped Timoshenko beams, International Journal of Engineering Science, 66 (2013) 1-13.

[24] M.-O. Belarbi, A.A. Daikh, A. Garg, T. Merzouki, H. Chalak, H. Hirane, Nonlocal finite element model for the bending and buckling analysis of functionally graded nanobeams using a novel shear deformation theory, Composite Structures, 264 (2021) 113712.

[25] D.C. Rodopoulos, T.V. Gortsas, S.V. Tsinopoulos, D. Polyzos, Numerical evaluation of strain gradients in classical elasticity through the Boundary Element Method, European Journal of Mechanics-A/Solids, 86 (2021) 104178.

[26] M. Mohammadimehr, M. Mehrabi, F.S. Mousavinejad, Magneto-mechanical vibration analysis of single-/three-layered micro-Timoshenko porous beam and graphene platelet as reinforcement based on modified strain gradient theory and differential quadrature method, Journal of Vibration and Control, (2020) 1077546320949083.

[27] J. Miglani, B. Devarajan, R.K. Kapania, Thermal buckling analysis of periodically supported composite beams using Isogeometric analysis, in: 2018 AIAA/ASCE/AHS/ASC Structures, Structural Dynamics, and Materials Conference, 2018, pp. 1224.

[28] S. Faroughi, E. Shafei, T. Rabczuk, Anisotropic solid-like shells modeled with NURBS-based isogeometric approach: Vibration, buckling, and divergence analyses, Computer Methods in Applied Mechanics and Engineering, 359 (2020) 112668.

[29] Y.-X. Zhen, S.-L. Wen, Y. Tang, Free vibration analysis of viscoelastic nanotubes under longitudinal magnetic field based on nonlocal strain gradient Timoshenko beam model, Physica E: Low-dimensional Systems and Nanostructures, 105 (2019) 116-124.

[30] A. Babaei, A. Rahmani, On dynamic-vibration analysis of temperature-dependent Timoshenko microbeam possessing mutable nonclassical length scale parameter, Mechanics of Advanced Materials and Structures, (2018) 1-8.

[31] R. Ansari, V. Mohammadi, M.F. Shojaei, R. Gholami, S. Sahmani, On the forced vibration analysis of Timoshenko nanobeams based on the surface stress elasticity theory, Composites Part B: Engineering, 60 (2014) 158-166.

[32] M. Simsek, Forced vibration of an embedded single-walled carbon nanotube traversed by a moving load using nonlocal Timoshenko beam theory, Steel and Composite Structures, 11(1) (2011) 59-76.

[33] Y. Gao, W.-s. Xiao, H. Zhu, Nonlinear vibration analysis of different types of functionally graded beams using nonlocal strain gradient theory and a two-step perturbation method, The European Physical Journal Plus, 134(1) (2019) 23.

[34] S. Rajasekaran, H. Bakhshi Khaniki, Finite element static and dynamic analysis of axially functionally graded nonuniform small-scale beams based on nonlocal strain gradient theory, Mechanics of Advanced Materials and Structures, (2018) 1-15.

[35] A. Aria, M. Friswell, A nonlocal finite element model for buckling and vibration of functionally graded nanobeams, Composites Part B: Engineering, 166 (2019) 233-246.

[36] L.C. Trinh, T.P. Vo, H.-T. Thai, T.-K. Nguyen, Size-dependent vibration of bi-directional functionally graded microbeams with arbitrary boundary conditions, Composites Part B: Engineering, 134 (2018) 225-245.

[37] F. Ebrahimi, M.R. Barati, Vibration analysis of nonlocal beams made of functionally graded material in thermal environment, The European Physical Journal Plus, 131(8) (2016) 279.

[38] F. Ebrahimi, M.R. Barati, Surface effects on the vibration behavior of flexoelectric nanobeams based on nonlocal elasticity theory, The European Physical Journal Plus, 132(1) (2017) 19.

[39] S.S. Mirjavadi, B. Mohasel Afshari, N. Shafiei, S. Rabby, M. Kazemi, Effect of temperature and porosity on the vibration behavior of two-dimensional functionally graded micro-scale Timoshenko beam, Journal of Vibration and Control, 24(18) (2018) 4211-4225.

[40] E.E. Ghandourh, A.M. Abdraboh, Dynamic analysis of functionally graded nonlocal nanobeam with different porosity models, Steel and Composite Structures, 36(3) (2020) 293-305.

[41] C. Roque, P. Martins, A. Ferreira, R. Jorge, Differential evolution for free vibration optimization of functionally graded nano beams, Composite Structures, 156 (2016) 29-34.

[42] N. Shafiei, S.S. Mirjavadi, B. MohaselAfshari, S. Rabby, M. Kazemi, Vibration of two-dimensional imperfect functionally graded (2D-FG) porous nano-/micro-beams, Computer Methods in Applied Mechanics and Engineering, 322 (2017) 615-632.

[43] A. Babaei, A. Rahmani, I. Ahmadi, Transverse vibration analysis of nonlocal beams with various slenderness ratios, undergoing thermal stress, Archive of Mechanical Engineering, (2019).

[44] Y. Yuan, K. Zhao, Y. Zhao, K. Kiani, Nonlocal-integro-vibro analysis of vertically aligned monolayered nonuniform FGM nanorods, Steel and Composite Structures, 37(5) (2020) 551-569.

[45] D. Srivastava, A phenomenological model of the rotation dynamics of carbon nanotube gears with laser electric fields, Nanotechnology, 8(4) (1997) 186.

[46] S. Zhang, W.K. Liu, R.S. Ruoff, Atomistic simulations of double-walled carbon nanotubes (DWCNTs) as rotational bearings, Nano Letters, 4(2) (2004) 293-297.

[47] R. Ansari, J. Torabi, Numerical study on the free vibration of carbon nanocones resting on elastic foundation using nonlocal shell model, Applied Physics A, 122(12) (2016) 1-13.

[48] H.B. Khaniki, Vibration analysis of rotating nanobeam systems using Eringen's two-phase local/nonlocal model, Physica E: Low-dimensional Systems and Nanostructures, 99 (2018) 310-319.

[49] H. Arvin, The flapwise bending free vibration analysis of micro-rotating timoshenko beams using the differential transform method, Journal of Vibration and Control, 24(20) (2018) 4868-4884.

[50] A. Babaei, C.X. Yang, Vibration analysis of rotating rods based on the nonlocal elasticity theory and coupled displacement field, Microsystem Technologies, 25(3) (2019) 1077-1085.

[51] J. Aranda-Ruiz, J. Loya, J. Fernández-Sáez, Bending vibrations of rotating nonuniform nanocantilevers using the Eringen nonlocal elasticity theory, Composite Structures, 94(9) (2012) 2990-3001.

[52] M. Ghadiri, N. Shafiei, Nonlinear bending vibration of a rotating nanobeam based on nonlocal Eringen's theory using differential quadrature method, Microsystem Technologies, 22(12) (2016) 2853-2867.

[53] S. Pradhan, T. Murmu, Application of nonlocal elasticity and DQM in the flapwise bending vibration of a rotating nanocantilever, Physica E: Low-dimensional Systems and Nanostructures, 42(7) (2010) 1944-1949.

[54] J. Fang, J. Gu, H. Wang, Size-dependent three-dimensional free vibration of rotating functionally graded microbeams based on a modified couple stress theory, International Journal of Mechanical Sciences, 136 (2018) 188-199.

[55] J. Fang, D. Zhou, Y. Dong, Three-dimensional vibration of rotating functionally graded beams, Journal of Vibration and Control, 24(15) (2018) 3292-3306.

[56] S. Bhattacharya, D. Das, Free vibration analysis of bidirectional-functionally graded and double-tapered rotating micro-beam in thermal environment using modified couple stress theory, Composite Structures, 215 (2019) 471-492.

[57] S. Yin, Y. Deng, G. Zhang, T. Yu, S. Gu, A new isogeometric Timoshenko beam model incorporating microstructures and surface energy effects, Mathematics and Mechanics of Solids, 25(10) (2020) 2005-2022.

[58] A. Norouzzadeh, R. Ansari, H. Rouhi, Nonlinear bending analysis of nanobeams based on the nonlocal strain gradient model using an isogeometric finite element approach, Iranian Journal of Science and Technology, Transactions of Civil Engineering, 43(1) (2019) 533-547.

[59] J. Ehyaei, A. Akbarshahi, N. Shafiei, Influence of porosity and axial preload on vibration behavior of rotating FG nanobeam, Advances in nano research, 5(2) (2017) 141.

[60] F. Ebrahimi, N. Shafiei, Application of Eringens nonlocal elasticity theory for vibration analysis of rotating functionally graded nanobeams, Smart Structures and Systems, 17(5) (2016) 837-857.

[61] H. Rouhi, F. Ebrahimi, R. Ansari, J. Torabi, Nonlinear free and forced vibration analysis of Timoshenko nanobeams based on Mindlin's second strain gradient theory, European Journal of Mechanics-A/Solids, 73 (2019) 268-281.

[62] M. Azimi, S.S. Mirjavadi, N. Shafiei, A. Hamouda, E. Davari, Vibration of rotating functionally graded Timoshenko nano-beams with nonlinear thermal distribution, Mechanics of Advanced Materials and Structures, 25(6) (2018) 467-480.

[63] M. Mohammadi, M. Safarabadi, A. Rastgoo, A. Farajpour, Hygro-mechanical vibration analysis of a rotating viscoelastic nanobeam embedded in a visco-Pasternak elastic medium and in a nonlinear thermal environment, Acta Mechanica, 227(8) (2016) 2207-2232.

[64] R. Talebitooti, S.O. Rezazadeh, A. Amiri, Comprehensive semi-analytical vibration analysis of rotating tapered AFG nanobeams based on nonlocal elasticity theory considering various boundary conditions via differential transformation method, Composites Part B: Engineering, 160 (2019) 412-435.

[65] X. Wang, Differential Quadrature and Differential Quadrature Based Element Methods, in, Elsevier, 2015.

[66] L. Behera, S. Chakraverty, Application of Differential Quadrature method in free vibration analysis of nanobeams based on various nonlocal theories, Computers & Mathematics with Applications, 69(12) (2015) 1444-1462.

[67] J. Reddy, Microstructure-dependent couple stress theories of functionally graded beams, Journal of the Mechanics and Physics of Solids, 59(11) (2011) 2382-2399.

Figures

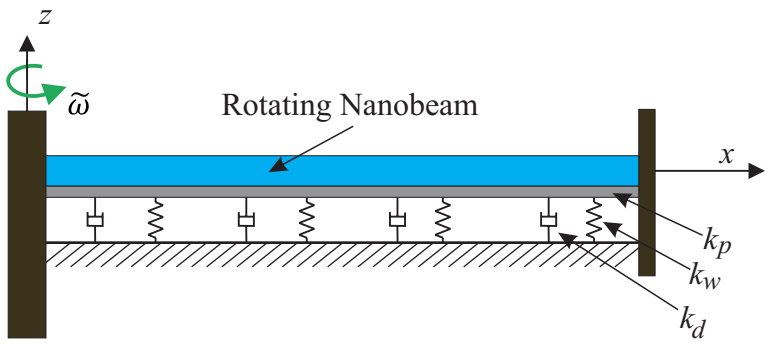

Fig. 1: Rotating Nanobeam Resting on a Winkler-Pasternak Foundation with CC Boundary Conditions

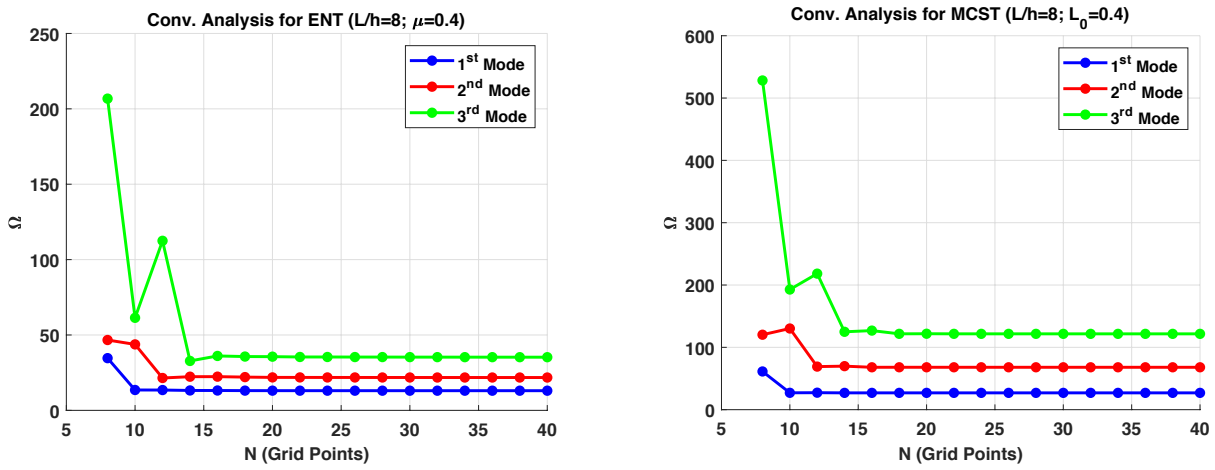

(a) Eringen's Nonlocal Theory (b) Modified Couple-Stress Theory

Fig. 2: Convergence analysis for DQM

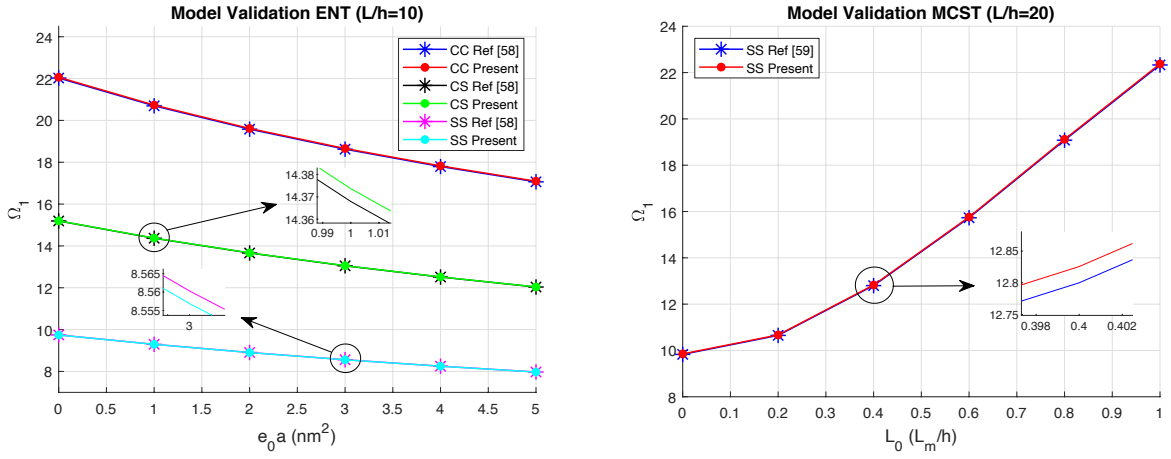

(a) ENT with Ref [58] (b) MCST with Ref [59]

Fig. 3: Verification the results of the proposed model

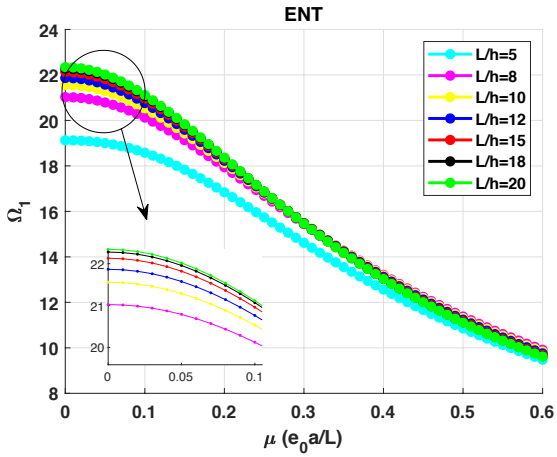

Fig. 4: Non-dimensional Fundamental Frequency for Different Slenderness Ratios (*L/h*) and versus the Nondimensional Nonlocal Parameter (ENT)

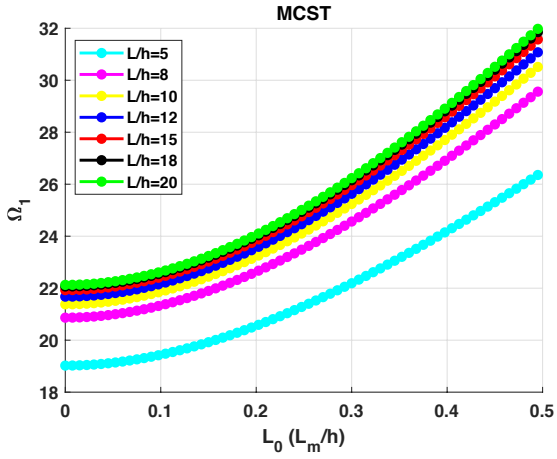

Fig. 5: Non-dimensional Fundamental Frequency for Different Slenderness Ratios (*L/h*) and versus the Length Scale Parameter (MCST)

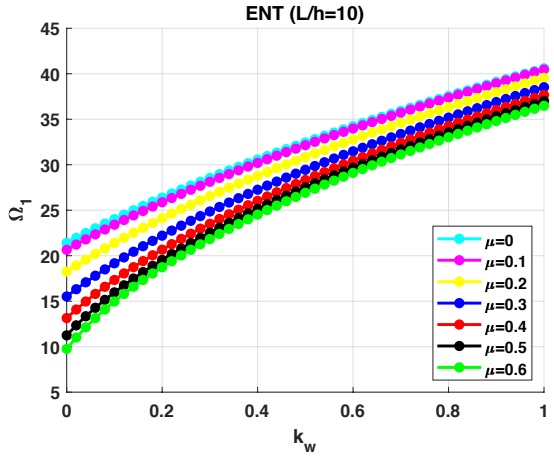

(a) Eringen's Nonlocal Theory, L/h=10

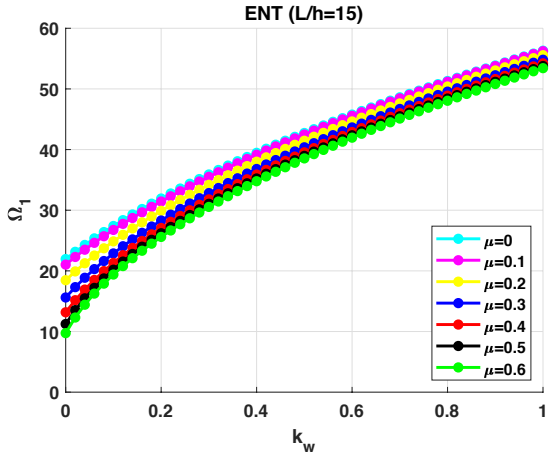

(b) Eringen's Nonlocal Theory, L/h=15

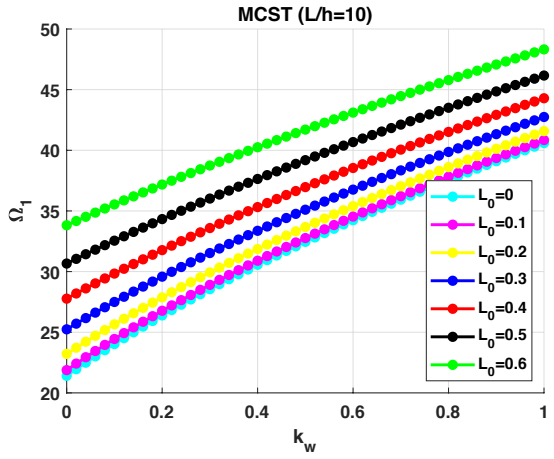

(c) Modified Couple-Stress Theory, L/h=10

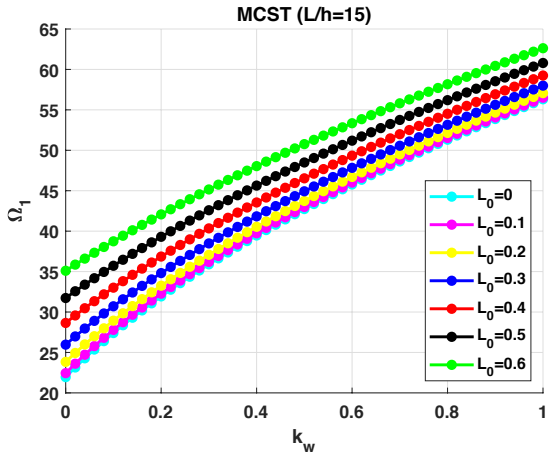

(d) Modified Couple-Stress Theory, L/h=15

Fig. 6: Non-dimensional Fundamental Frequency for Different Slenderness Ratios (L/h) and versus the Winkler Coefficients

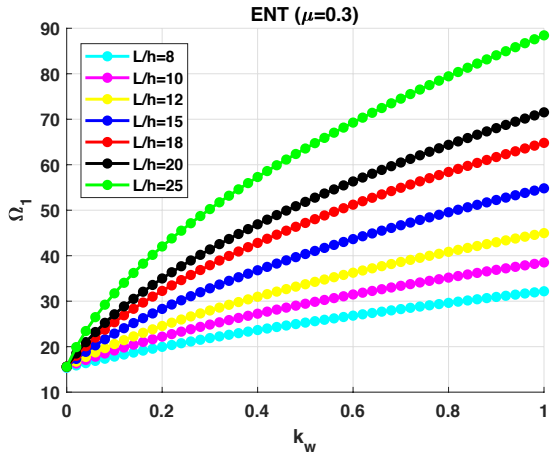

(a) Eringen's Nonlocal Theory, μ=0.3

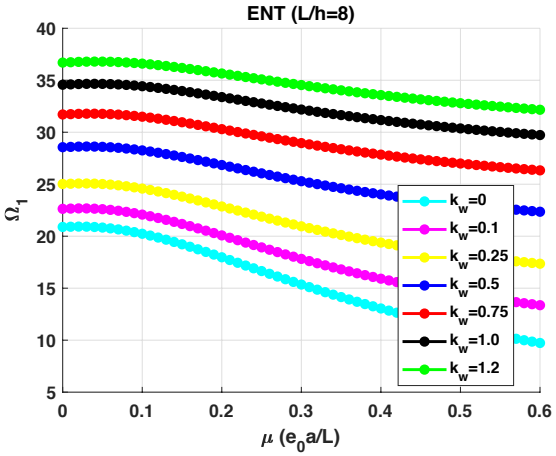

(b) Eringen's Nonlocal Theory, *L/h*=8

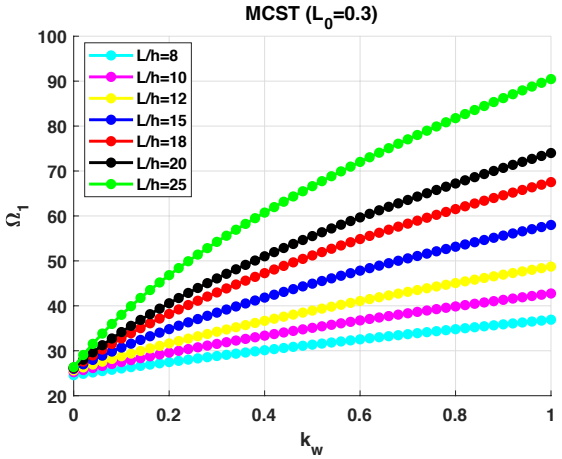

(c) Modified Couple-Stress Theory, $L_0 = 0.3$

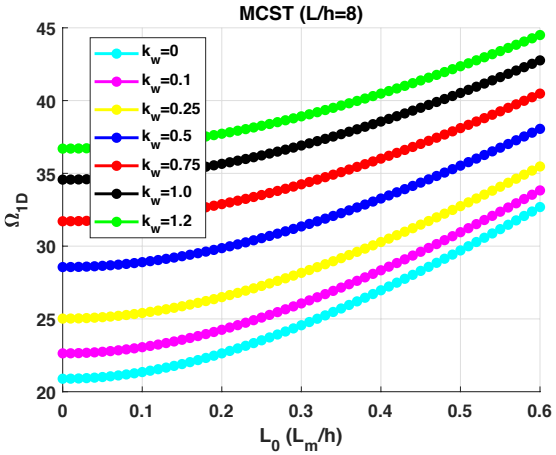

(d) Modified Couple-Stress Theory, *L/h*=8

Fig 7: Simultaneous Effect of Slenderness Ratio and Winkler Coefficient on the Non-dimensional Fundamental Frequency

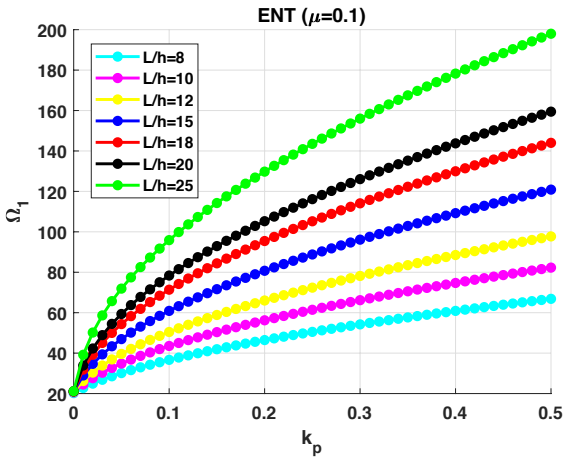

(a) Eringen's Nonlocal Theory, μ=0.1

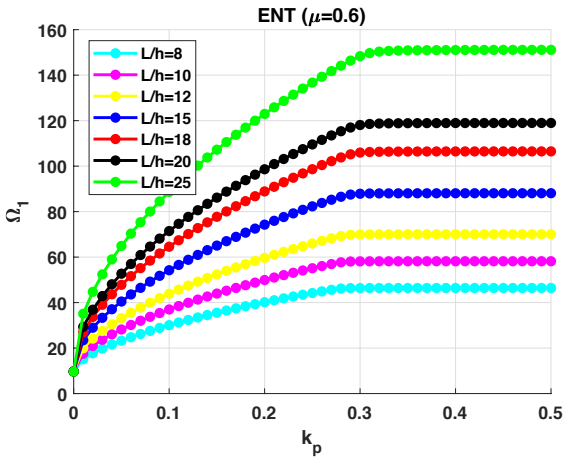

(b) Eringen's Nonlocal Theory, μ=0.6

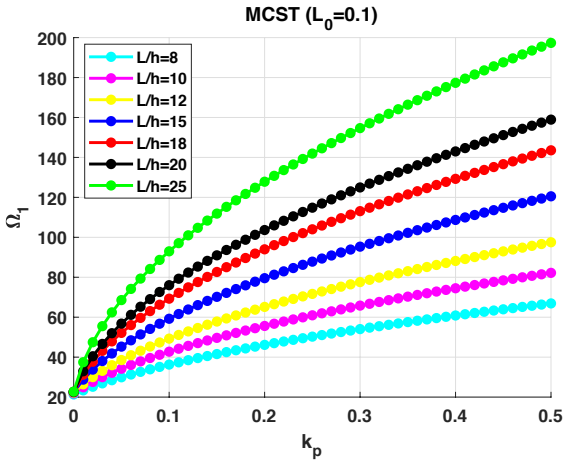

(c) Modified Couple-Stress Theory, $L_0 = 0.1$

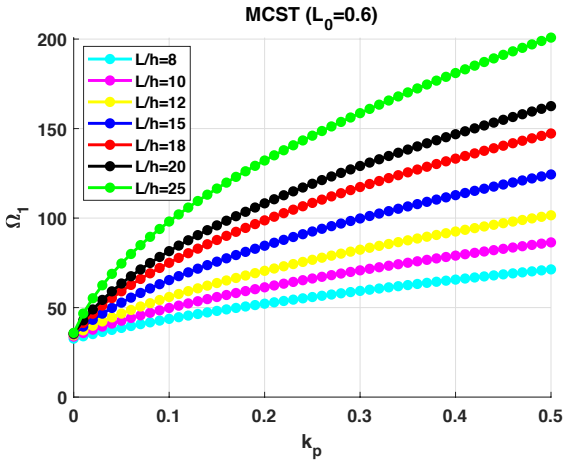

(d) Modified Couple-Stress Theory, $L_0 = 0.6$

Fig. 8: Non-dimensional Fundamental Frequency for Different Slenderness Ratios and versus the Pasternak Coefficient

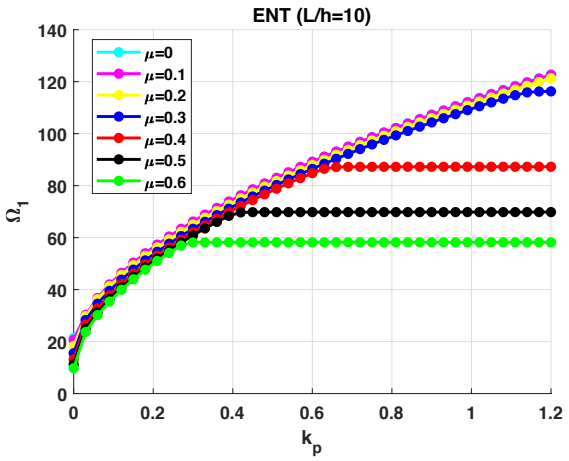

(a) Eringen's Nonlocal Theory, *L/h*=10

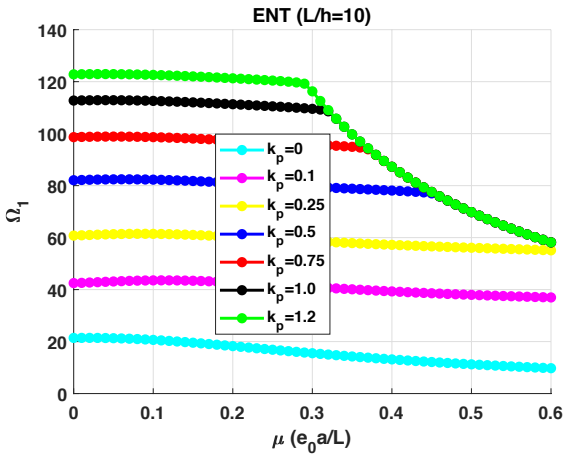

(b) Eringen's Nonlocal Theory, *L/h*=10

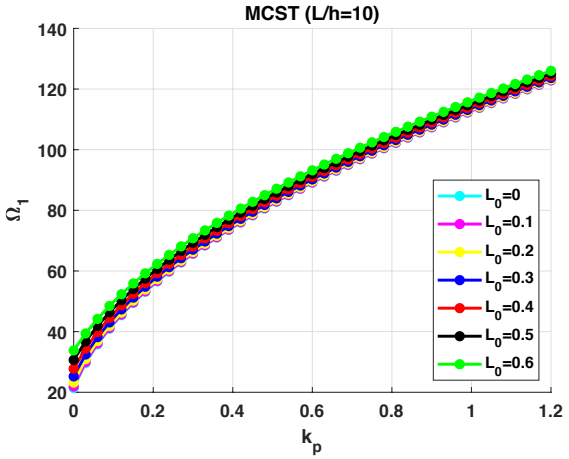

(c) Modified Couple-Stress Theory, *L/h*=10

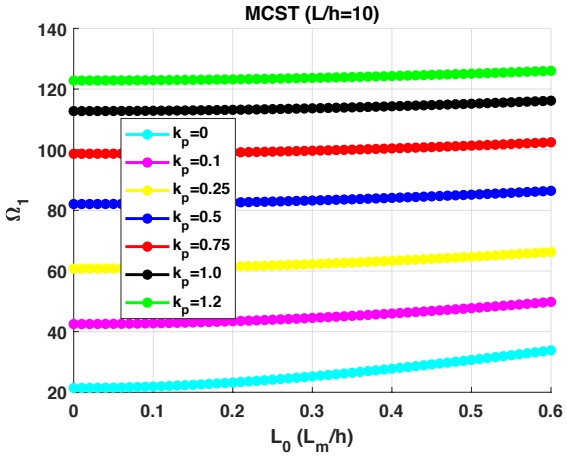

(d) Modified Couple-Stress Theory, *L/h*=10

Fig. 9: Effect of Pasternak Coefficients on the Non-dimensional Fundamental Frequency

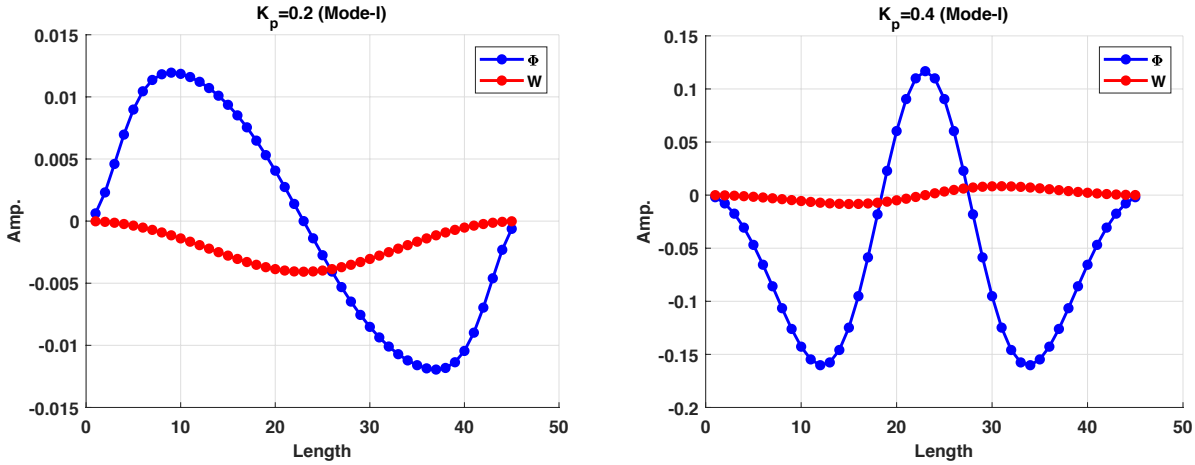

(a) Pasternak Coefficient, $k_p = 0.2$ (b) Pasternak Coefficient, $k_p = 0.4$

Fig. 10: Fundamental Mode Shapes for Eringen's Nonlocal Theory with *L/h*=10

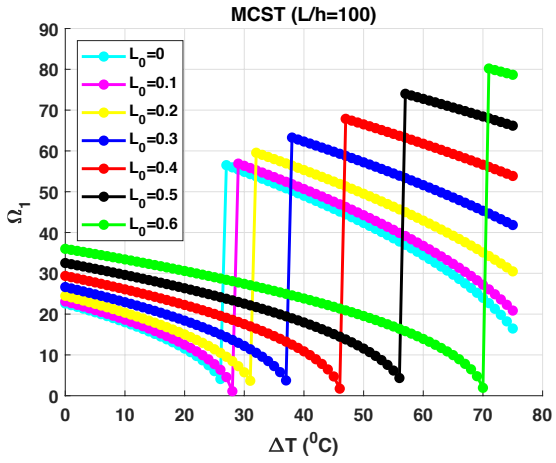

Fig. 11: The Fundamental Non-Dimensional Frequency versus the Variation of Temperature for Different Length Scales

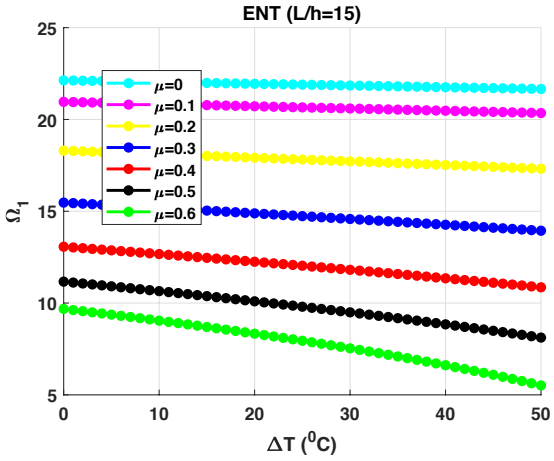

(a) Eringen's Nonlocal Theory, *L/h*=15

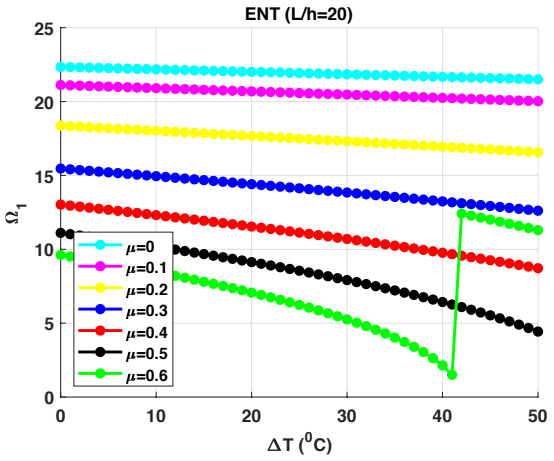

(b) Eringen's Nonlocal Theory, *L/h*=20

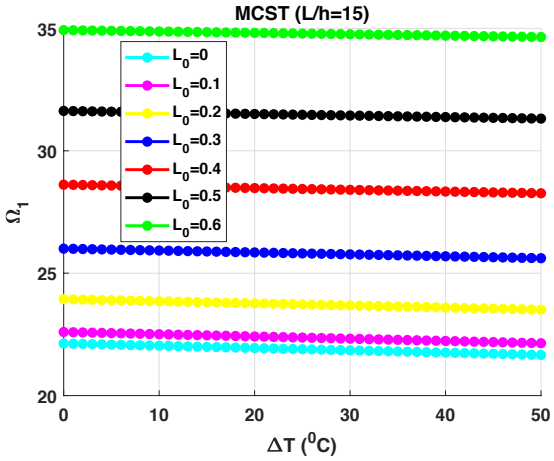

(c) Modified Couple-Stress Theory, *L/h*=15

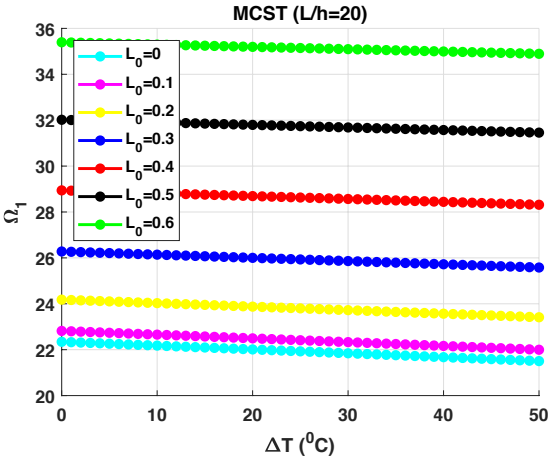

(d) Modified Couple-Stress Theory, *L/h*=20

Fig. 12: Non-Dimensional Fundamental Frequency versus the Variation of Temperature

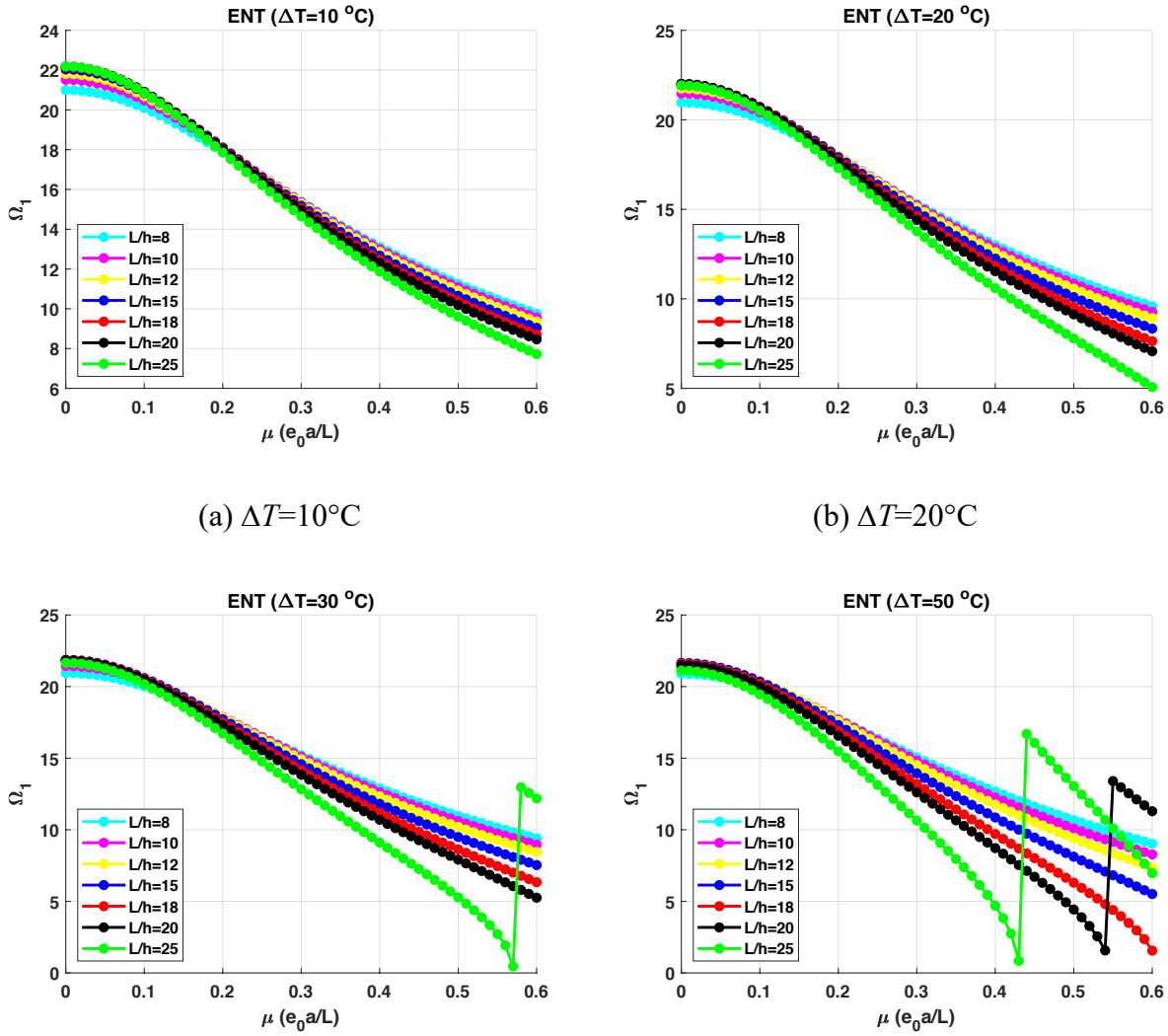

(a) ΔT=10°C

(b) ΔT=20°C

(c) ΔT=30°C

(d) ΔT=40°C

Fig. 13: Effect of Temperature Gradient and Nonlocal Parameters on Non-Dimensional Fundamental Frequency for Eringen's Nonlocal Theory

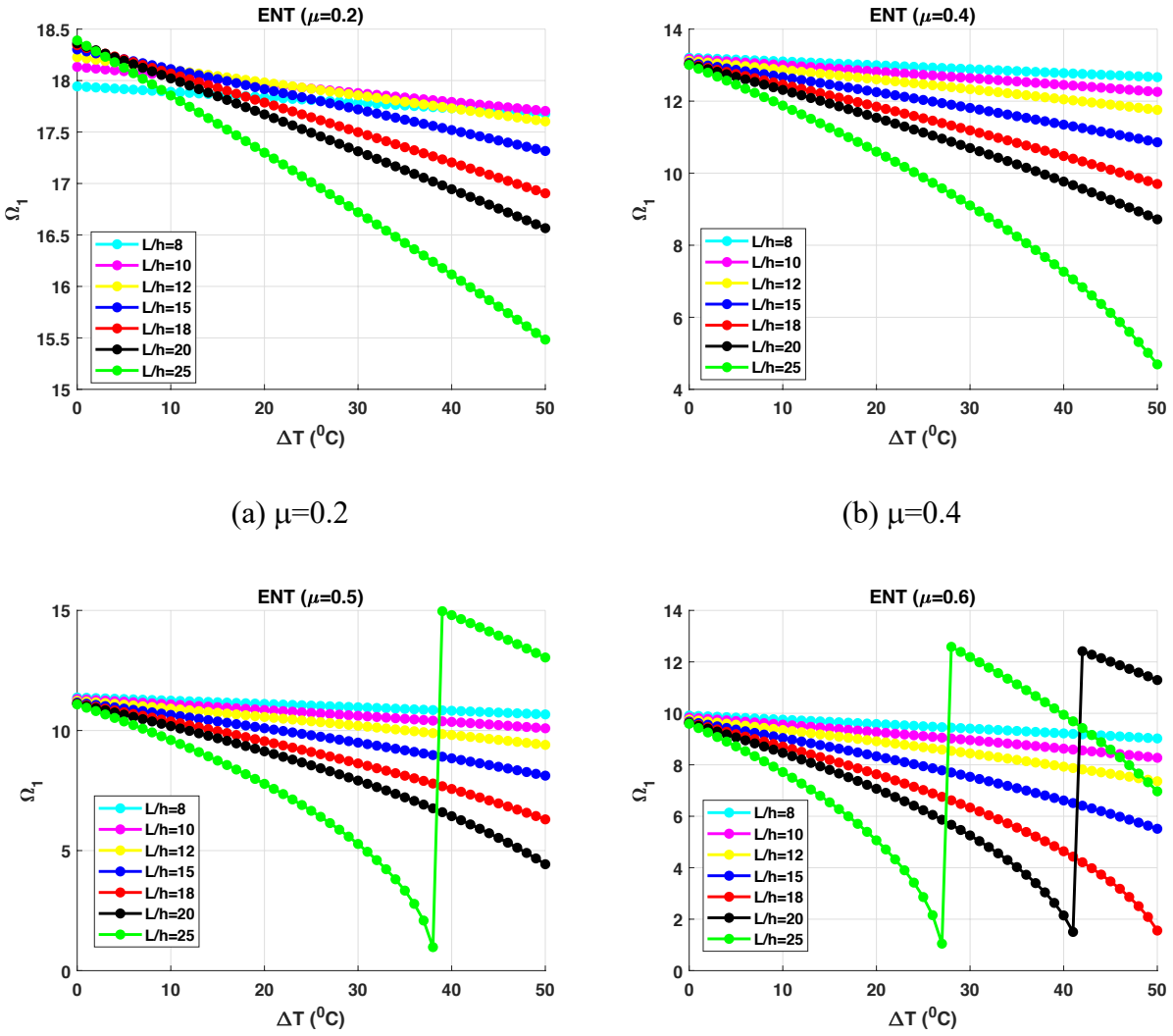

(a) μ=0.2

(b) μ=0.4

(c) μ=0.5

(d) μ=0.6

Fig. 14: Simultaneous Effect of the Slenderness Ratio and Temperature Gradient on the Non-Dimensional Fundamental Frequency for Eringen's Nonlocal Theory

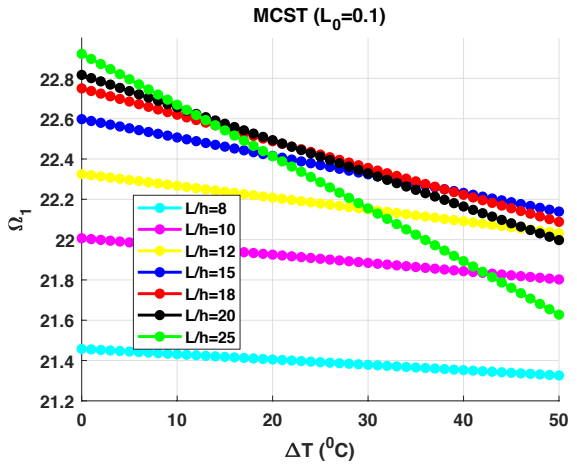

(a) $L_0 = 0.1$

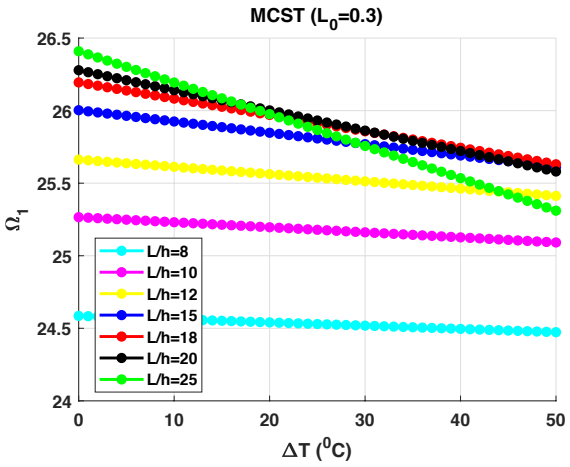

(b) $L_0 = 0.3$

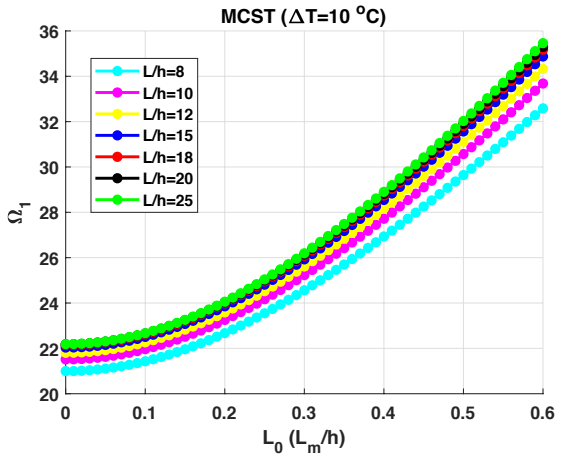

(c) ΔT=10°C

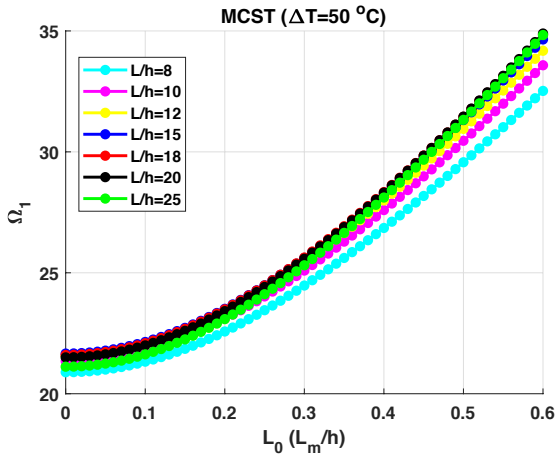

(d) ΔT=50°C

Fig. 15: Simultaneous Effect of the Slenderness Ratio and Temperature on the Non-Dimensional Frequency Based on Modified Couple-Stress Theory

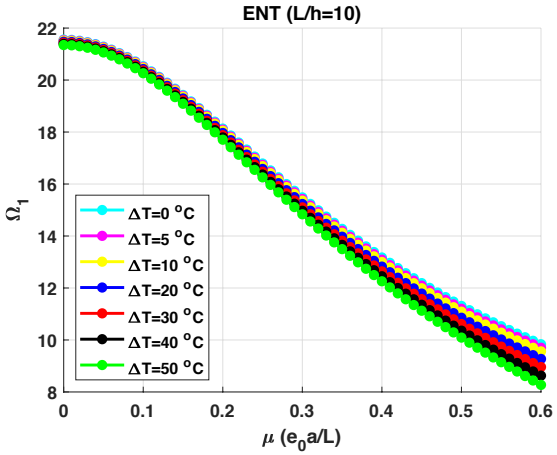

(a) Eringen's Nonlocal Theory, versus Nonlocal Parameter for L/h=10

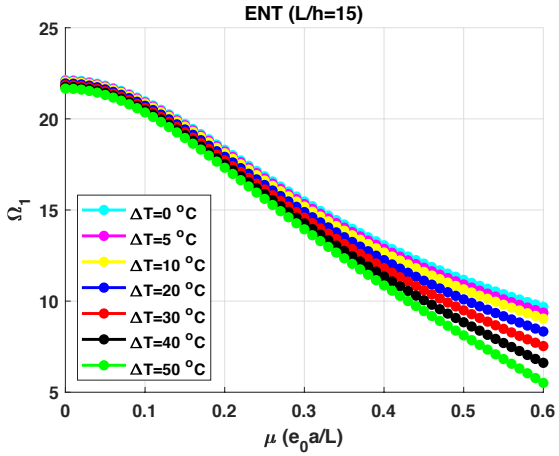

(b) Eringen's Nonlocal Theory, versus Nonlocal Parameter for L/h=15

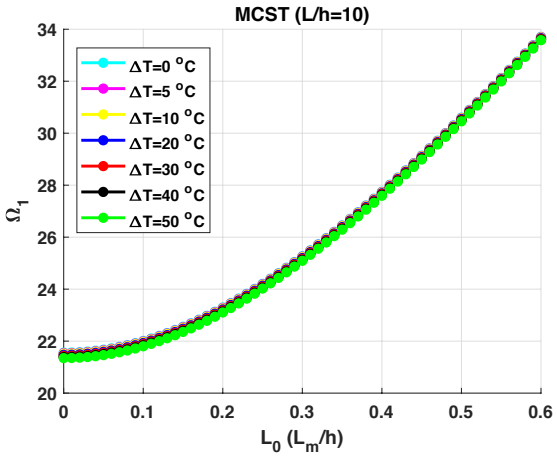

(c) Modified Couple-Stress Theory, versus Length Scale for L/h=10

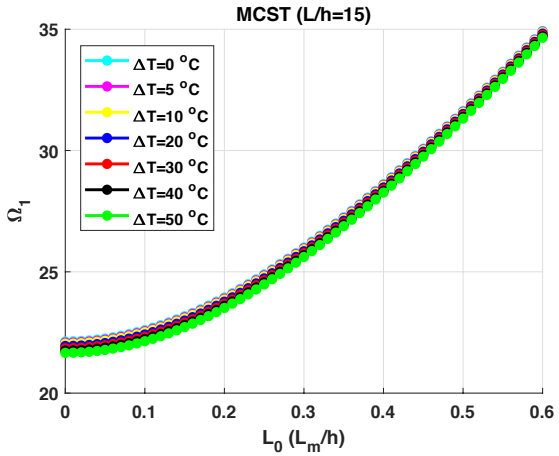

(d) Modified Couple-Stress Theory, versus Length Scale for L/h=15

Fig. 16: Non-Dimensional Fundamental Frequency for Different Temperature Gradients

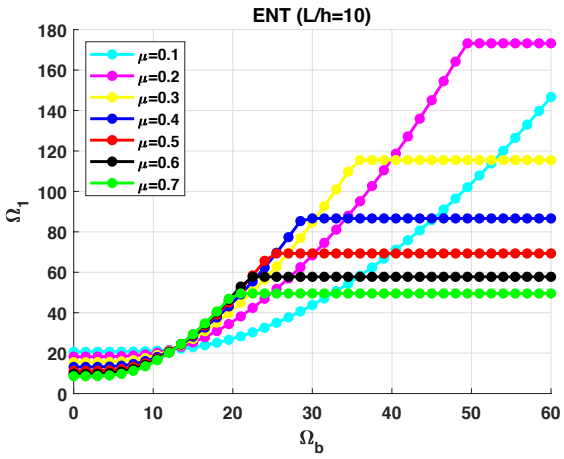

(a) Eringen's Nonlocal Theory, versus Nonlocal Parameter for L/h=10

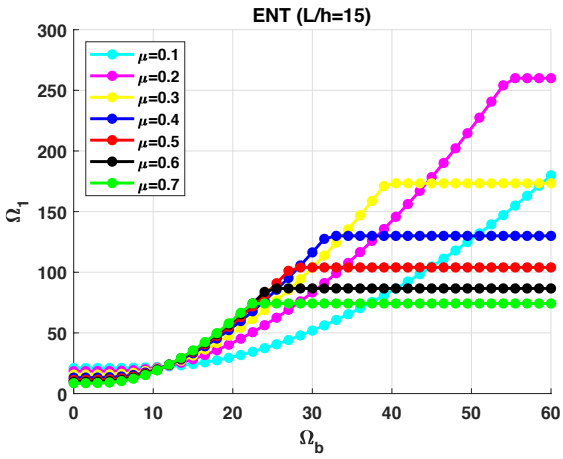

(b) Eringen's Nonlocal Theory, versus Nonlocal Parameter for L/h=15

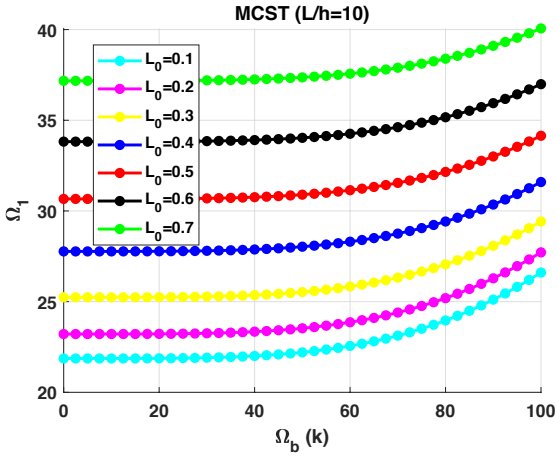

(c) Modified Couple-Stress Theory, versus Length Scale for L/h=10

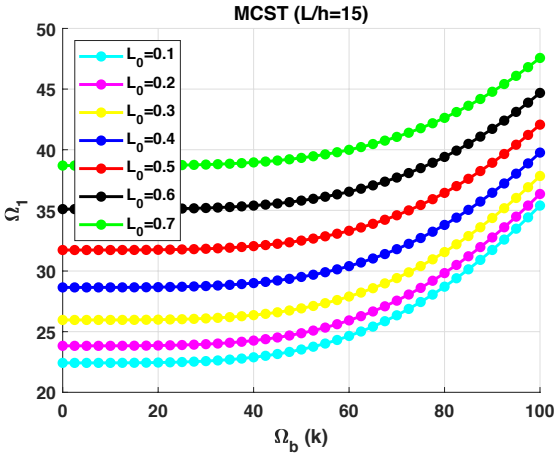

(d) Modified Couple-Stress Theory, versus Length Scale for L/h=15

Fig. 17: Non-Dimensional Fundamental Frequency versus Rotating Velocity of the Nano-Beam

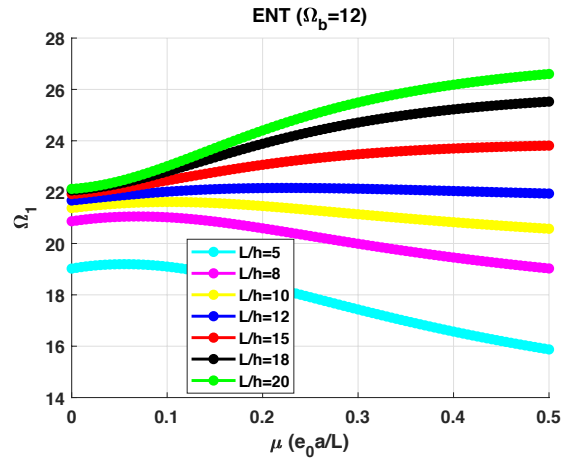

(a) $\Omega_b = 12$

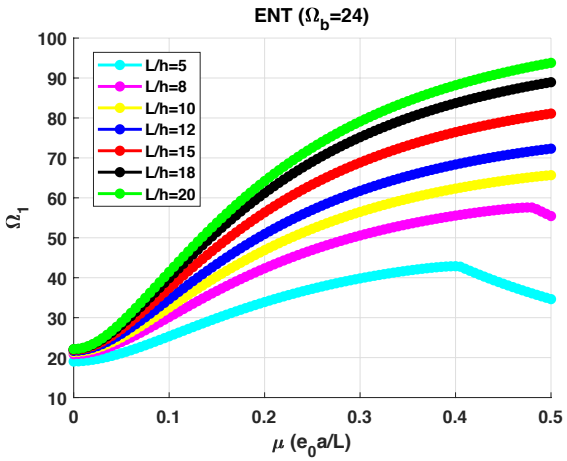

(b) $\Omega_b = 24$

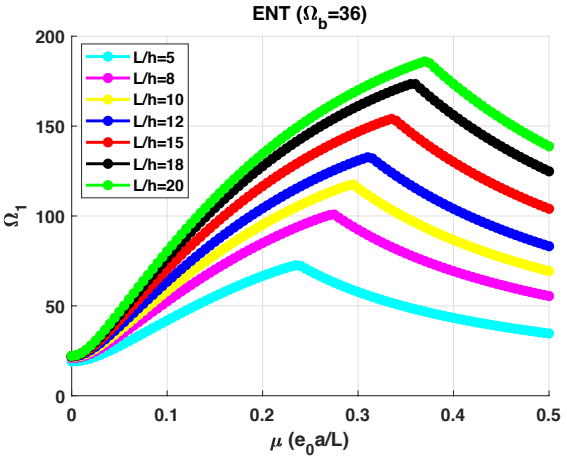

(c) $\Omega_b = 36$

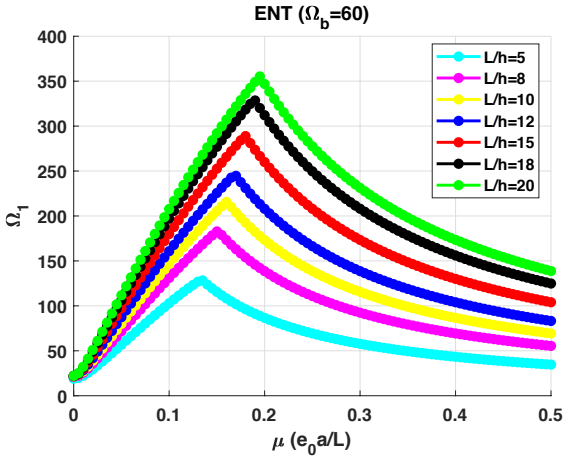

(d) $\Omega_b = 60$

Fig 18: Simultaneous Effect of Slenderness Ratio and Rotating Velocity of the Nano-Beam on the Non-Dimensional Fundamental Frequency for Eringen's Nonlocal Theory

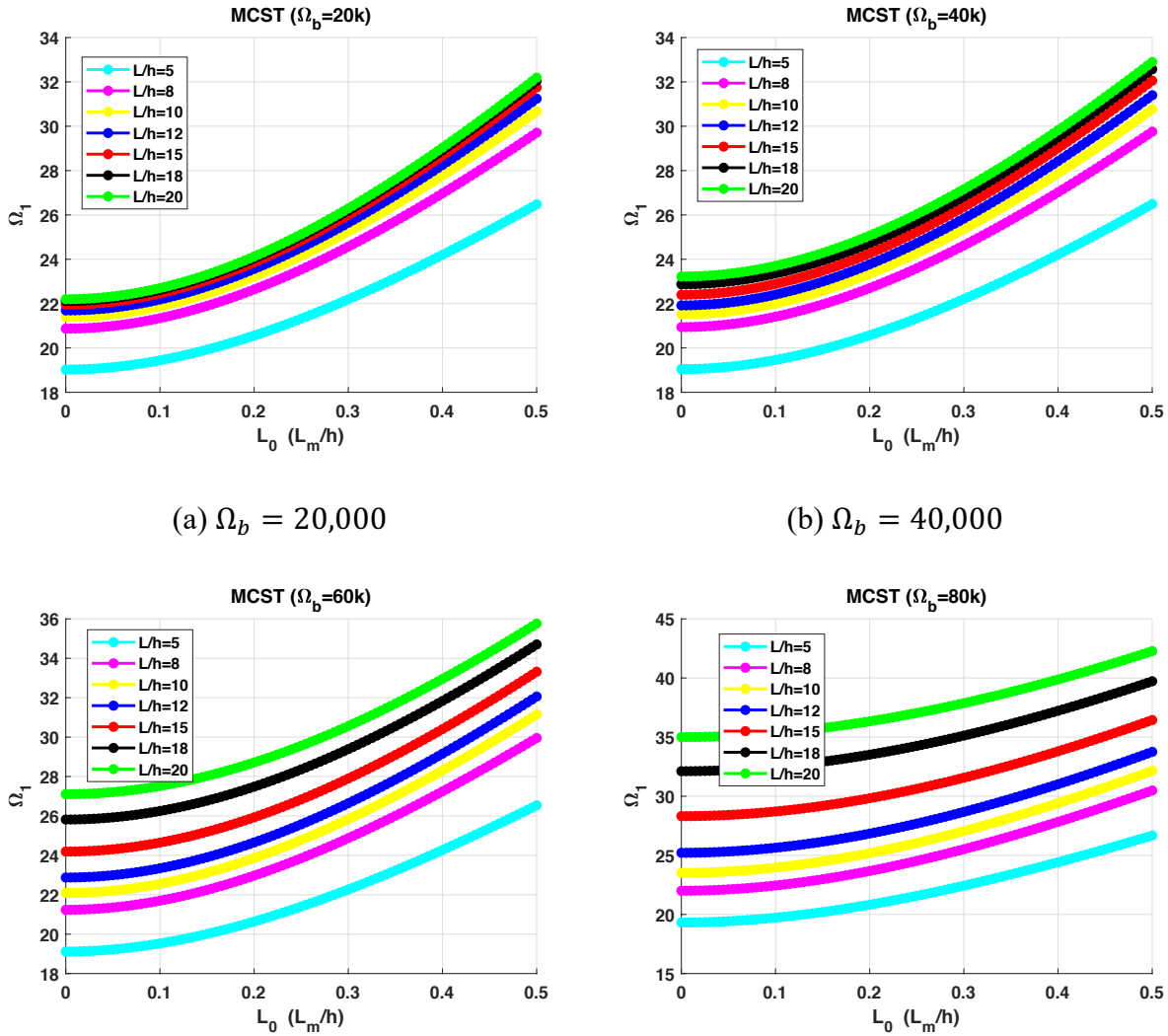

(a) $\Omega_b = 20{,}000$

(b) $\Omega_b = 40{,}000$

(c) $\Omega_b = 60{,}000$

(d) $\Omega_b = 80{,}000$

Fig 19: Simultaneous Effect of Slenderness Ratio and Rotating Velocity of the Nano-Beam on the Non-Dimensional Fundamental Frequency for Modified Couple-Stress Theory

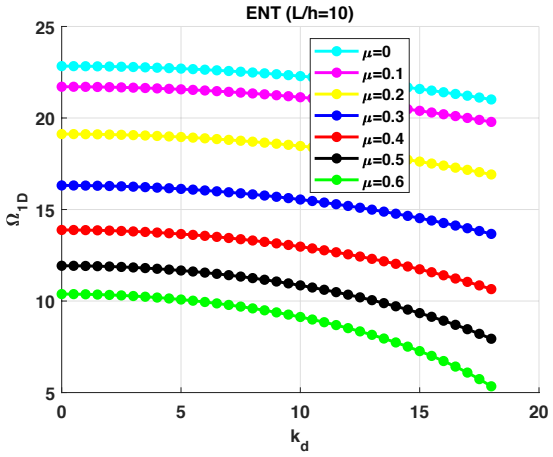

(a) Non-Dimensional Damped Natural Frequency

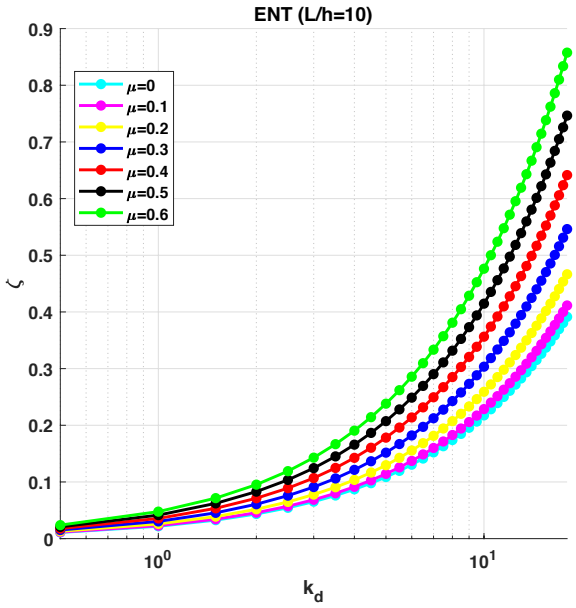

(b) Damping Ratio

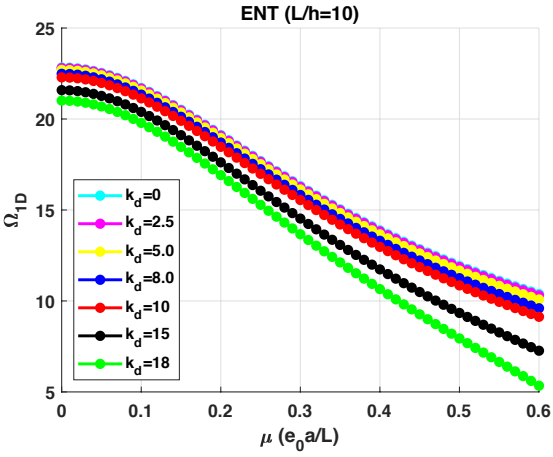

(c) Non-Dimensional Damped Natural Frequency

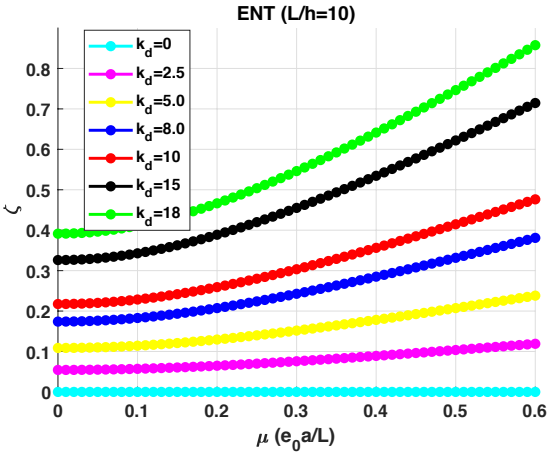

(d) Damping Ratio

Fig 20: Effect of the Visco-Elastic Foundation on the Dynamics of the Nanobeam for Eringen's Nonlocal Theory for *L/h*=10 and Different Nonlocal Parameters and Visco-Elastic Coefficient

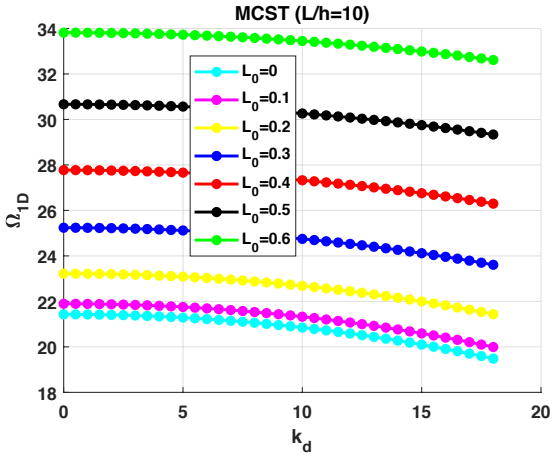

(a) Non-Dimensional Damped Natural Frequency

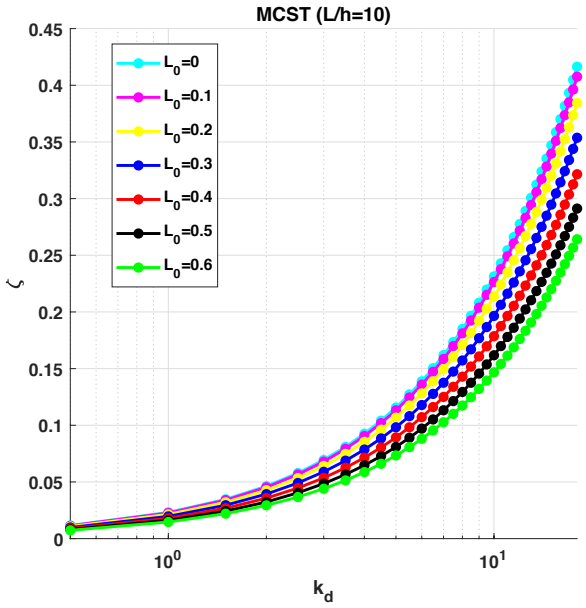

(b) Damping Ratio

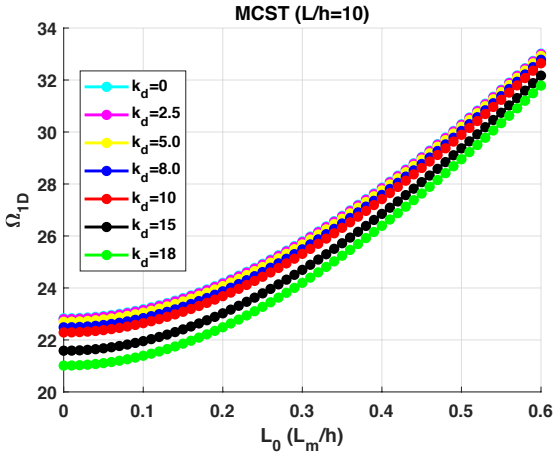

(c) Non-Dimensional Damped Natural Frequency

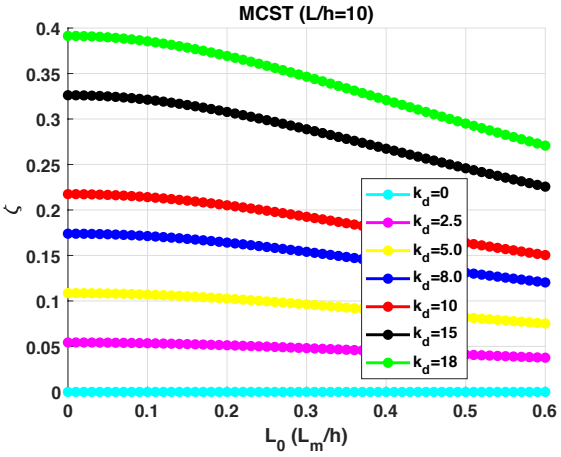

(d) Damping Ratio

Fig 21: Effect of the Visco-Elastic Foundation on the Dynamics of the Nanobeam for Modified Couple Stress Theory for *L/h*=10 and Different Length Scale Parameters and Visco-Elastic Coefficient

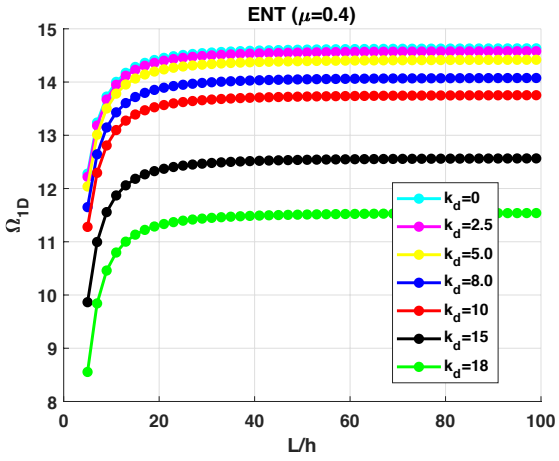

(a) Eringen's Nonlocal Theory, Non-Dimensional Damped Natural Frequency, μ=0.4

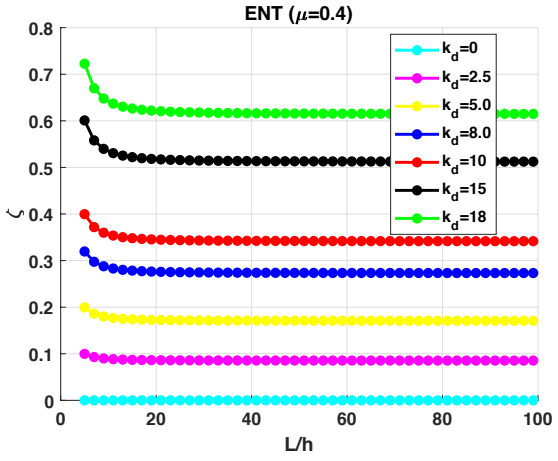

(b) Eringen's Nonlocal Theory, Damping Ratio, μ=0.4

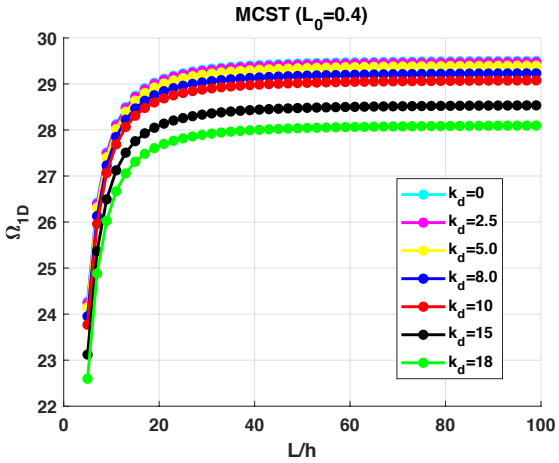

(c) Modified Couple Stress Theory, Non-Dimensional Damped Natural Frequency, $L_0 = 0.4$

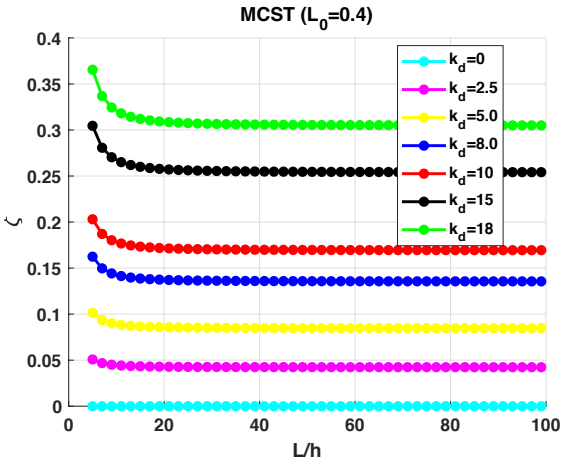

(d) Modified Couple Stress Theory, Damping Ratio, $L_0 = 0.4$

Fig 22: Simultaneous Effect of the Visco-Elastic Foundation and Slenderness Ratio on the Dynamics of the Nanobeam

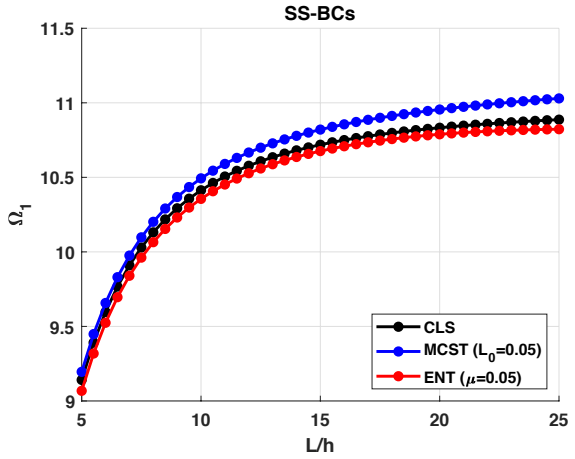

(a) SS BCs

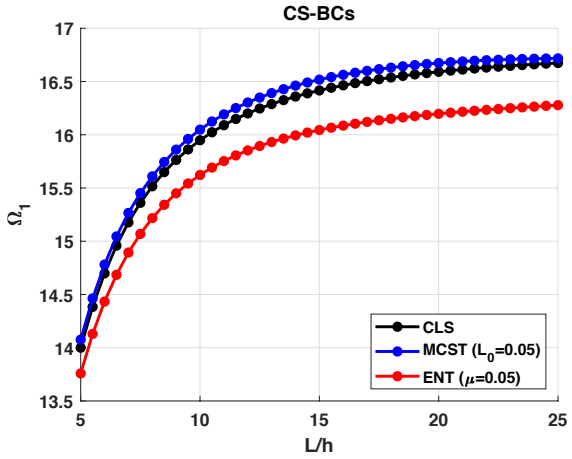

(b) CS BCs

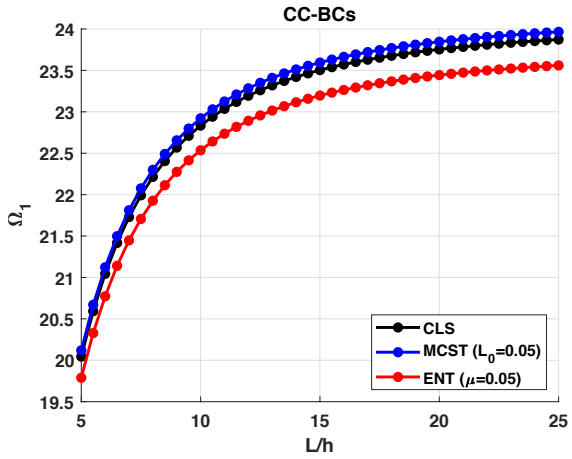

(c) CC BCs

Fig. 23: Effects of Boundary Conditions on Non-Dimensional Natural Frequency